Toward More Cost-Effective and Greener Chemicals Production from Shale Gas by Integrating with Bioethanol Dehydration: Novel Process Design and Simulation-Based Optimization

Chang He
Dept. of Chemical and Biological Engineering, Northwestern University, Evanston, IL 60208

State Key Laboratory of Heavy Oil Processing, College of Chemical Engineering, China University of Petroleum, Beijing 102249, China

Fengqi You
Dept. of Chemical and Biological Engineering, Northwestern University, Evanston, IL 60208

DOI 10.1002/aic.14713
Published online December 30, 2014 in Wiley Online Library (wileyonlinelibrary.com)

A novel process design for a more cost-effective, greener process for making chemicals from shale gas and bioethanol is presented. The oxidative coupling of methane and cocracking technologies are considered for converting methane and light natural gas liquids, into value-added chemicals. Overall, the process includes four process areas: gas treatment, gas to chemicals, methane-to-ethylene, and bioethanol-to-ethylene. A simulation-optimization method based on the NSGA-II algorithm for the life cycle optimization of the process modeled in the Aspen HYSYS is developed. An energy integration model is also fluidly nested using the mixed-integer linear programming. The results show that for a "good choice" optimal design, the minimum ethylene selling price is \$655.1/ton and the unit global-warming potential of ethylene is 0.030 kg CO_2-eq/kg in the low carbon shale gas scenario, and \$877.2/ton and 0.360 kg CO_2-eq/kg in the high carbon shale gas scenario. *AIChE J*, 61: 1209–1232, 2015
Keywords: shale gas, chemicals, natural gas liquids, simulation-optimization, global-warming potential

Introduction

Driven by advances in technology such as hydraulic fracturing and horizontal drilling, shale gas production in North America has increased rapidly in recent years. The Potential Gas Committee estimated that the United States possesses nearly 2700 trillion standard cubic feet (tscf) of potential natural gas, 40% of which is extractable shale gas.[1] At the current consumption rates of 23 tscf per year, this potential amounts to 47 years worth of fuel. This increasing production will also make natural gas more affordable in the United States, benefitting the petrochemical, refining, and midstream industries by providing low-cost energy. In particular, shale gas is a potential "game-changer" in the chemical industry, due to its ability to be used in the production of olefins.[2] Olefins are important intermediates in the commodity chemical value chain, as they can be used to produce value-added chemicals like plastics, synthetic rubber, adhesives, and so forth.[3] Historically, the global production of ethylene has exceeded that of any other organic compound. Yet, a bright future for shale gas in the chemical industry is far from assured. Three major challenges that need to be addressed are listed below.[3,4]

Natural gas liquids and chemicals production

Shale gas is somewhat unique, as most of the shale gas resources in the United States are reported to be natural gas liquid (NGLs)-rich. For example, the Bakken shale gas produces a gas with super-rich NGLs content (20–40 mol %), and is believed to have the highest heat content among North American natural gas formations. After raw shale gas is purified and fractionated, the NGLs typically have substantially higher market values than methane.[5] Light NGLs, such as ethane, propane, and butanes (i-C_4 and n-C_4 hydrocarbons) can be used as feedstocks to produce olefins, while the remaining heavier fractions (C_{5+} hydrocarbons, named natural gasoline) can be used as gasoline blending stocks. Currently, in the United States, 99% of NGLs-derived ethane is used as a raw material in cracking facilities because it is cheaper and cleaner than petroleum-derived feedstocks (such as naphtha). However, due to high transportation costs and safety concerns, the majority of NGLs compounds, especially ethane, are not suitable for long-distance transportation, and most end-use markets for NGL products are stagnant. Hence, the excessive supply of NGLs has become an issue in regions lacking in abundant NGLs processing and cracking facilities.[3] Most recently, He and You[6] proposed three novel process designs for integrating shale gas

Additional Supporting Information may be found in the online version of this article.

Correspondence concerning this article should be addressed to F. You at you@northwestern.edu.

processing with on-site ethylene production. The economic evaluation proves that the NGLs-richer shale gas generally results in net present values (NPVs) that are 3.17–5.12 times higher than those of a NGLs-leaner gas.

Breaking C—H single bonds in methane

Methane is always the dominant ingredient in the shale gas, making up typically 75−90% of the total gas. However, methane has high C—H bond strength (434 kJ/mol) and a large ionization energy, making it difficult to break.[7] The current industrial practice of steam reforming (SMR, see Eq. 1) produces syngas, which can be further used as an intermediate to produce synthetic hydrocarbons. Such indirect syngas-based routes have been investigated in recent years. EI-Halwagi and coworkers[8,9] addressed process integration and performed techno-economic and environmental impact analyses of a shale gas-to-methanol plant. Martín and Grossmann[10] presented a superstructure optimization approach for the simultaneous production of liquid fuels and hydrogen from a hybrid shale gas and switchgrass process. However, these routes have been criticized for having high production and capital costs, large CO_2 emissions, and low carbon-atom utilization efficiency.[7]

Direct, one-step conversion of methane to value-added chemicals and fuels is potentially more economical and environmentally friendly. In the pioneering work by Keller and Bhasin in the early 1980s,[11] methane was activated with the assistance of oxygen and further converted into ethylene and ethane; this process came to be known as the oxidative coupling of methane (OCM, see Eq. 2) reaction. This finding attracted global attention. Most of the previous works were oriented toward finding a suitable catalyst for selective methane conversion. Unfortunately, a standalone OCM process has very little economic potential compared to well-established cracking facilities.[12] The major limitations of the OCM process are its low C_2 hydrocarbons yield (ethane and ethylene, <20 mol %) and selectivity (<50%) with large amounts of unreacted gas and by-product. These disadvantages result in high product separation costs, poor low project economics, and inevitably heavy carbon footprint. Recently, the maximum C_2 hydrocarbons yield of 13.6 mol % was achieved for a fixed-bed OCM reactor using response surface methodology.[13] Godini et al.[12] have analyzed the techno-economic performance of an OCM process by integration with a methane reforming process, resulting in a 35 mol % C_2 hydrocarbons yield and a 60% total methane conversion. Siluria Technologies announced that they had developed an approach allowing for industrial-scale OCM process by discovering a biotemplate and nanowire catalyst.[14] Among these reports, effectively recovering unreacted CH_4 from the OCM reactor effluent and integrating other endothermic processes are promising solutions. Nevertheless, the associated by-product separation and carbon footprint issues have not been well addressed yet

$$CH_4 + H_2O \xrightarrow{SMR} CO + H_2(\text{syngas}) \rightarrow .... \rightarrow C_mH_n \quad (1)$$

$$CH_4 + O_2 \xrightarrow{OCM} C_mH_n + CO_2 + CO + H_2 \quad (2)$$

Life cycle greenhouse gas emissions reduction

The recent growth in shale gas production has also resulted in increasing concerns about the environmental impacts (climate change, water, etc.).[15–19] One concern of particular interest is the potential environmental footprint of the increased fugitive CH_4 emissions during drilling.[20] However, two almost opposing points have been proposed regarding whether shale gas is a low carbon fuel or not.[21] The dispute was initiated because quantitatively assessing the leaking data of CH_4 is complex and varies from well to well, potentially leading to serious environmental issues. To date, there is no research that considers the greenhouse gas (GHG) mitigation of chemicals production from shale gas. Typically, adding a carbon capture and sequestration (CCS) process is a direct approach to reduce the process CO_2 emission. Additionally, from a sustainability point of view, the life cycle GHG emissions can be inherently mitigated by incorporating a renewable biofuel as a hybrid feedstock.[10,22] As a first generation biofuel, corn-derived bioethanol is an ideal choice, as it is currently commercially available, and bioethylene production via bioethanol dehydration (BD) is prevalent in the United States and Brazil.[23,24] More importantly, BD involves a strong endothermic reaction which is fueled by natural gas in industrial practices. The low heating value (LHV) of this dehydration fuel is equivalent to about 5% of that of bioethanol.[25] In this regard, a new opportunity arises because the shale gas-based chemical production process has an abundance of methane and other fuel gases. They can be fluidly integrated together, and the amount of bioethanol fed can be flexibly adjusted according to the desired life cycle GHG emissions reduction of the entire process.

In light of the aforementioned challenges, this work presents an innovative process design for more cost-effective and greener chemicals production from a hybrid shale gas and bioethanol system. The process integrates cocracking of light NGLs, the OCM reaction, and BD with raw shale gas processing. Correspondingly, the proposed process consists of four process areas, namely gas treatment, gas to chemicals, methane to ethylene, and bioethanol to ethylene. The key novelties of this process design are: (1) thermal conversion of complete C_1, C_2, and C_3 fractions to chemicals; (2) a complex coprocessing strategy to purify and separate gas products including the OCM product and cocracking gas with raw shale gas; (3) this work reflects the first attempt to address the mitigation of life cycle GHG emissions for shale gas-based chemical processes using CCS and sustainable integration of bioethylene production. Based on rigorous process modeling, a simulation-optimization method based on a nondominated sorting genetic algorithm (NSGA-II) for life cycle optimization (LCO) of the proposed process is developed. In addition, an energy integration model is also fluidly nested in the simulation-optimization using mixed-integer linear programming (MILP). The method is applied to simultaneously conduct a techno-economic analysis, an environmental impact analysis, and energy integration. This is a complex problem due to the considerable amount of decision variables and built-in unit specifications/parameters (e.g., basic operating conditions in column design) involved in the optimization models and in the HYSYS simulation, as well as a set of design and operational constraints that must be satisfied. To tackle this problem, we systematically describe the general methodology and strategy for better convergence and computation time reduction. In addition, considering the controversy of GHG emissions associated with shale gas production, we adopt two life cycle assessment scenarios in the LCO model, namely low carbon shale gas (LCSG) and high

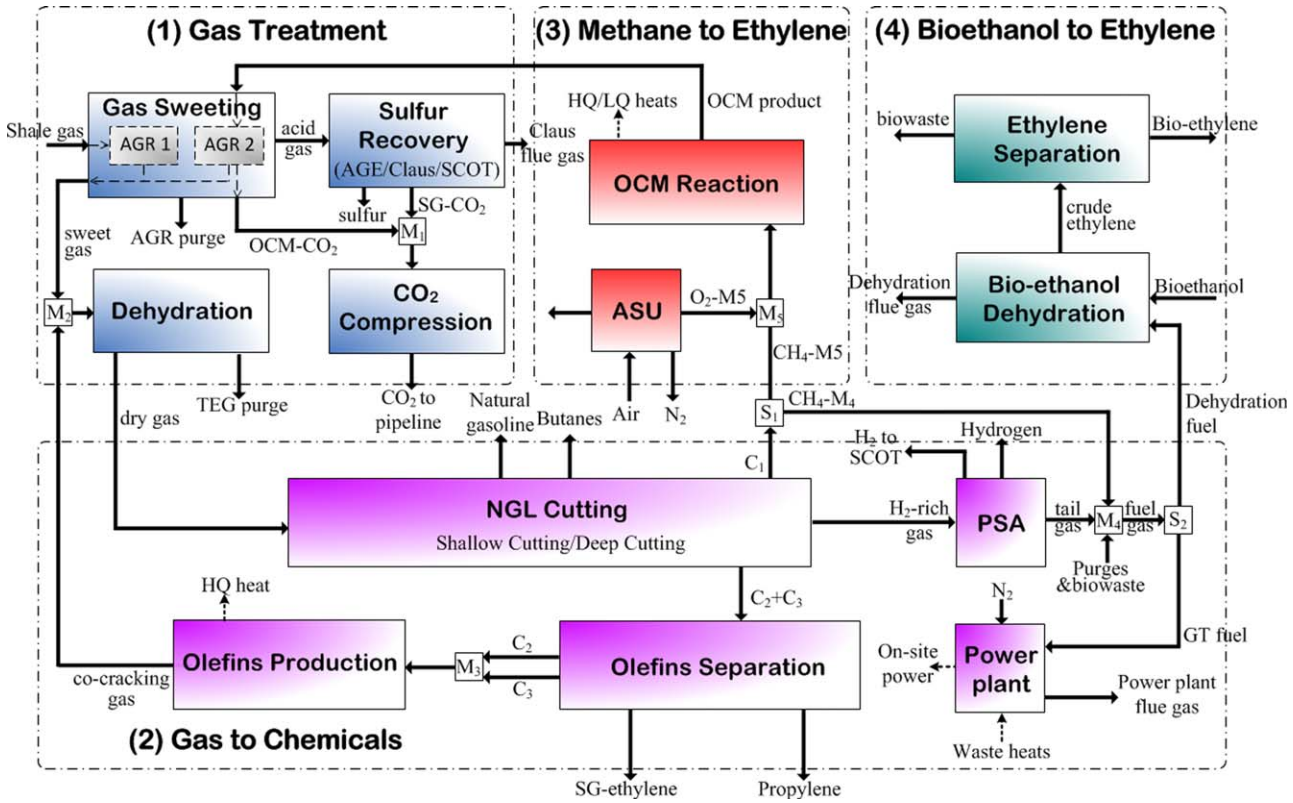

Figure 1. Simplified representation of shale gas/bioethanol to chemicals process.

[Color figure can be viewed in the online issue, which is available at wileyonlinelibrary.com.]

carbon shale gas (HCSG). For both scenarios, this simulation-optimization approach provides optimal process designs and decision variables, and clearly presents the Pareto trade-off between the NPV and global-warming potential (GWP).

Process Description

A chemicals production process from shale gas integrated with BD is shown in Figure 1. Briefly, the overall process includes four process areas below. (1) The gas treatment area, where the raw shale gas and OCM product are purified in a gas sweetening unit. The H_2S in the removed acid gas is converted into sulfur in a sulfur recovery unit. The acidic CO_2 (SG-CO_2), along with the OCM-derived CO_2 (OCM-CO_2) is collected at point M_1 and is then compressed into the liquid phase in a CO_2 compression unit. The CO_2 liquid is transported through pipelines to sequestration sites. Once purified, the sweet gas is mixed with cocracking gas at point M_2. The mixture is dried in a dehydration unit and then processed in the (2) gas-to-chemicals area. In this area, the heavy NGLs (butanes and natural gasoline) and low-boiling point gases (methane and H_2-rich gas) are successively taken from the dry gas using a NGLs cutting unit. The C_2 and C_3 hydrocarbons included in the remaining stream are sent to an olefins separation unit where the olefin products are separated from the light NGLs. In the next step, the ethane and propane are mixed at point M_3 and then thermally cocracked in an olefins production unit. Meanwhile, a pressure swing adsorption (PSA) unit is used to recover high-quality hydrogen from the H_2-rich gas. The rejected PSA tail gas is mixed with process purges (acid gas removal (AGR) and Triethylene glycol (TEG) purges), a portion of methane (from point S_1), and biowaste at point M_4. The mixture passes through the point S_2 where the upper branch goes to the (4) bioethanol-to-ethylene area as dehydration fuel, and the lower branch is sent to power plant as gas turbine (GT) fuel. We note that all process waste heat is integrated within this power plant to generate power using the Rankine cycle. The next area is the (3) methane-to-ethylene area, where the incoming methane (from point S_1) is partially oxidized via the OCM reaction in an O_2-rich environment. The OCM product includes ethylene, ethane, hydrogen, carbon dioxide, carbon monoxide, water, and a large quantity of unconverted methane, which is obtained from the first two process areas. As mentioned in Introduction, bioethanol can be used as a renewable feedstock introduced to the (4) bioethanol-to-ethylene Area. In the BD unit, the input amount of bioethanol is fully dependent on that of furnace fuel, that is, by the split ratio at point S_2. The produced crude ethylene is purified via passing through a series of distillations in the ethylene separation unit. In this article, SG-ethylene and bioethylene refer to the ethylene produced from shale gas, and bioethanol, respectively.

For the calculations presented in this work, the shale gas is supplied at 60.0 bar, 35°C, and at a rate of 2000 kmol/h, with a LHV thermal input of 2093 GJ/h, based on normalized data reported from Eagle Ford formation (see Table A1 in Appendix).[26] Note that almost no literature explicitly provides the H_2S and H_2O content of shale gas. H_2S content is reported typically varying at a low H_2S/CO_2 molar ratio,[27] so it is assumed to be 0.5 for the H_2S/CO_2 in this study. The moisture content associated with phase equilibrium is

Table 1. Assumptions Used in Process Simulation

	Values	Reference
Property Package		
Global	Peng–Robinson	
Local 1-Gas sweeting	Amine-KE	
Local 2-TEG dehydration	Glycol	
Solvent Concentration		
Lean DEA	0.4 g/g solvent	28
Lean MDEA	0.5 g/g solvent	29
Lean TEG	1.0 g/g solvent	30
CO_2 Compression		
LP/MP/HP	1.7/21/80 bar	31
Supercritical Pressure	153 bar	31
OCM reactor		
Heat losses	2.5%	–
CSTR numbers/volume	1/see Figure 5	
Cocracking Reactor		
Heat losses	2.5%	–
CSTR numbers/volume	10/30 m^3	–
Steam/$C_2 + C_3$ hydrocarbons	0.4 kg/kg	32
Furnace (Claus/GT/Dehydration)		
Heat losses	1.5%	31,33
Compressor, Turbine, and Pump		
Adiabatic efficiency	0.72	34
Mechanical efficiency	1	34
Maximum outlet/inlet pressure ratio	5	34
Steam Cycle and GT		
LP/MP/HP steam pressure	29/60/125 bar	31,33
Condense pressure	0.1 bar	31,33
Maximum steam cycle temperature	550°C	31,33
Maximum GT outlet temperature	1377°C	31,33
Energy Integration		31,33
Boiler pressure	80/160 bar	31,33
Condense pressure	0.1 bar	28
Turbine inlet pressure	500/550 bar	31,33,35
Minimum temperature approach	10°C	36
Rankine cycle number	2	33,37
Heat exchanger maximum temperature	800°C	13,33

predicted using a correlation-based method developed by Bahadori et al.[28] Simulations were performed in Aspen HYSYS V7.2, using the Peng–Robinson equation globally. The Aspen HYSYS model, consisting of chemical reactions and unit operations, thermodynamic property methods and local properties, and process simulation and synthesis, is based on open literature reports and expert interviews. Major assumptions used throughout the simulation are summarized in Table 1. The following sections describe the simulation model in detail.

Gas treatment area

Gas Sweetening. In the gas sweetening unit, two acid gas removal (AGR) sections are used in parallel to purify the shale gas and the OCM product. Note that methane is used as an intermediate in this process, rather than as a final product (i.e., pipeline gas) in typical gas processing plants. Thus, some strict quality specifications (heat content, dew point, impurities content, etc.) on pipeline gas are not necessarily fulfilled. We simply focus on key factors including the technological feasibility, capacity, and requirements of downstream processing technologies. For example, to avoid potential freezing problems, the CO_2 concentration in the feed gas of the NGLs cutting and olefins separation processes should reside between 0.01 and 2.00 mol %.[38] In addition, the H_2S concentration should not exceed 50 ppm to prevent the OCM catalysts from being poisoned.[30]

We use chemical absorption-based AGR technology to remove acid gases, as shown by Figure 2 (1.1). A small amount of acid gas including H_2S and CO_2 is first taken away from the raw shale gas in the AGR1 section. Diethanol amine (DEA) is used as a solvent here because it can unselectively and effectively react with both H_2S and CO_2. In Figure 2 (1.1.1), most H_2S and CO_2 in the raw shale gas are absorbed by the lean solvent as it passes through the AGR1 absorber. The effluent from the absorber bottom containing rich DEA (38 wt %) passes through a pressure relief valve followed by a knock out (K.O.) drum to remove gaseous light hydrocarbons (0.1–0.3 mol/h), and then is depressurized to 2.1 bar via another valve. After that, the rich DEA stream is preheated to 78°C at a cross heat exchanger (cross-HX) by cooling the lean solvent exiting from the bottom of the AGR1 stripper. A stream of DEA solvent is regenerated in this stripper where the acid components dissolved in the rich solvent are stripped in the overhead acid gas. The regenerated DEA solvent along with makeup DEA/water is pumped to the first tray of the AGR1 absorber. After treatment in the AGR process, the H_2S and CO_2 concentrations are reduced to 4 ppm and 0.05 mol % in the sweet gas, respectively.

The other feed gas is the OCM product stream which contains about 20–30 mol % of CO_2, most of which must be rejected via a similar AGR process, shown in Figure 2 (1.1.2). Note that the off-gases from the top of the AGR1 and AGR2 absorbers are both sent to a condenser at 35°C to remove the liquid fraction, and the resulting sweet gas is processed in the next dehydration unit.

TEG Dehydration. After being purified in the gas sweetening unit, the entrained water in the sweet gas must be reduced to less than 0.1 ppm by dehydration to prevent hydrate formation and corrosion. TEG is by far the most common liquid desiccant used in the natural gas industry as it exhibits most of the desirable criteria of commercial suitability (e.g., high absorption efficiency and boiling point).[39] Herein, we use a centralized, enhanced TEG dehydration process, shown in Figure 2 (1.2). First, the sweet gas, mixed with cocracking gas, flows into a TEG contactor where it is countercurrently contacted and dried by rich TEG at roughly 29.0 bar. Next, 99.9% of the dry gas exiting from the contactor top is sent to the next NGLs cutting unit, and the remaining gas is sent to a surge tank as stripping gas. The enriched TEG solvent leaving from the contactor bottom is throttled to 2.8 bar and then preheated to 150°C in a cross-HX. Then, it flows through a TEG till (stripper) to regenerate TEG solvent. The TEG till overhead is cooled down to 25°C in a condenser where the resulting vapor is sent to point M_4 as a fuel. To enhance TEG recovery, we introduce a modified surge tank to further strip off water from the TEG stream. The surge tank uses a small amount of dry gas (0.5–2 mol/h) as stripping gas, reducing the vapor partial pressure of water. This lowers the water concentration in lean TEG stream from 1.0–5.0 wt % to less than 0.3 wt %. After being mixed with makeup TEG, the regenerated lean TEG stream is recycled to a TEG contactor at 30.0 bar and 50.0°C.

Sulfur Recovery. The acid gas contains low H_2S content (<40 mol %) and has a high CO_2/H_2S molar ratio (3.0–8.0), making it unsuitable for sulfur recovery using the Claus process directly.[29] An acid gas enrichment (AGE) process with a selective methyl-diethanolamine (MDEA) solvent is able to provide a higher H_2S content gas, as shown in Figure 2

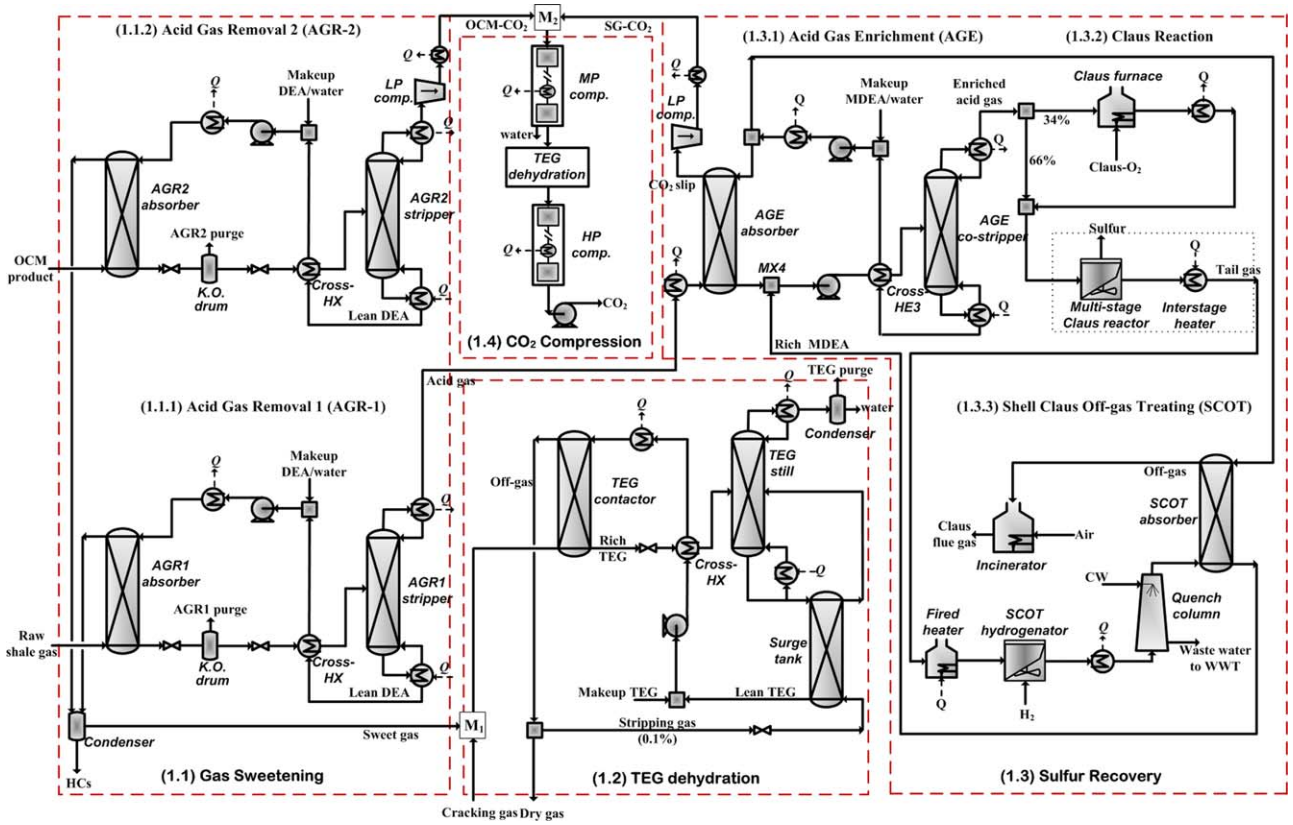

Figure 2. Flow sheet of gas treatment area.

(1.1) gas sweeting; (1.2) TEG dehydration; (1.3) sulfur recovery and (1.4) CO_2 compression. [Color figure can be viewed in the online issue, which is available at wileyonlinelibrary.com.]

(1.3.1). This is because the equilibrium solubility of H_2S in MDEA is much higher than that of CO_2.[40] Similarly to the AGR process, the feed gas is upgraded in an absorber-stripper process, where the AGE absorber operates at 0.5 bar. The MDEA solvent preferentially absorbs the H_2S and allows 60–80 mol % of the rejected CO_2 to remain in the CO_2 slip. Note that the CO_2 slip leaving the AGE absorber containing 90 mol % CO_2 is compressed to 11 bar at point M_2 for further CO_2 compression. Next, the AGE stripper can cotreat the rich solvent drawn back from the shell Claus off-gas treating (SCOT) absorber. After the AGE process, the enriched acid gas containing 75.0–80.0 mol % H_2S is sent to a Claus sulfur recovery section, shown in Figure 2 (1.3.2). To meet the stoichiometric requirement of the Claus reaction, a slight excess of O_2 produced from the air separation unit (ASU) is added to oxidize 34.0% of H_2S to SO_2, shown by Eq. 3. The produced SO_2 reacts with the oxidized H_2S in the bypassed acid gas to yield sulfur, which is a by-product (see Eq. 4). The Claus tail gas contains a small amount of H_2S (0.5–2.0 mol %) which needs to be removed via a SCOT process, see Figure 2 (1.3.3). In the SCOT process, the tail gas is first heated to the reaction temperature (300°C) before entering a catalytic hydrogenation reactor, which converts 99.9% of SO_2 to H_2S (see Eq. 5). The reactor effluent is condensed to 35°C by sequentially passing through a heater and a quench column with spraying water. The blowdown from the column bottom is sent to a waste water treatment unit for further degrading. The H_2S content (about 5 mol %) present in the quench column overhead gas is rejected in the SCOT absorber by contacting with the lean solvent regenerated from AGE section. Finally, the produced off-gas containing a small amount of H_2S (<50 ppm) goes to an incinerator, and the resulting Claus flue gas (about 70 mol % of CO_2) is directly discharged to the atmosphere

$$H_2S + 3/2O_2 \leftrightarrow SO_2 + H_2O \quad (3)$$

$$2H_2S + SO_2 \leftrightarrow 3S + 2H_2O \quad (4)$$

$$3H_2 + SO_2 \leftrightarrow H_2S + 2H_2O \quad (5)$$

CO_2 Compression. The CO_2 must be compressed to supercritical pressure in order to be ready for sequestration. In this unit, the OCM-CO_2 stream is mixed with the SG-CO_2 stream at point M_2, and the LP mixture (11 bar) is compressed to the MP (medium pressure) CO_2 at 21 bar by a multistage MP compressor. Two intercooled stages with K.O. drums are used for cooling and removing above 90% of water present in the feed stream. The remaining water is totally removed by a TEG dehydration section, which has the same process configuration with the TEG dehydration process shown in Figure 2 (1.2). The rejected water in this unit is collected in the liquid phase and recycled for steam generation. After that, the dehydrated CO_2 stream is further compressed to the liquid phase at 80 bar by a two-stage HP (high pressure) compressor. Finally, the CO_2 liquid is compressed to supercritical pressure (153 bar) for distribution in the CO_2 pipeline. The CO_2 is recovered at a high purity (98.5 mol %) with sufficiently low water (150 ppm), sulfur (100 ppm), and methane (0.5 mol %) contents that are well below NETL specifications.[41]

Gas-to-chemicals area

NGLs Cutting. For NGLs cutting (or NGLs recovery), cryogenic separation is a cost-effective approach that uses a refrigeration system to partially liquefy the dry gas.

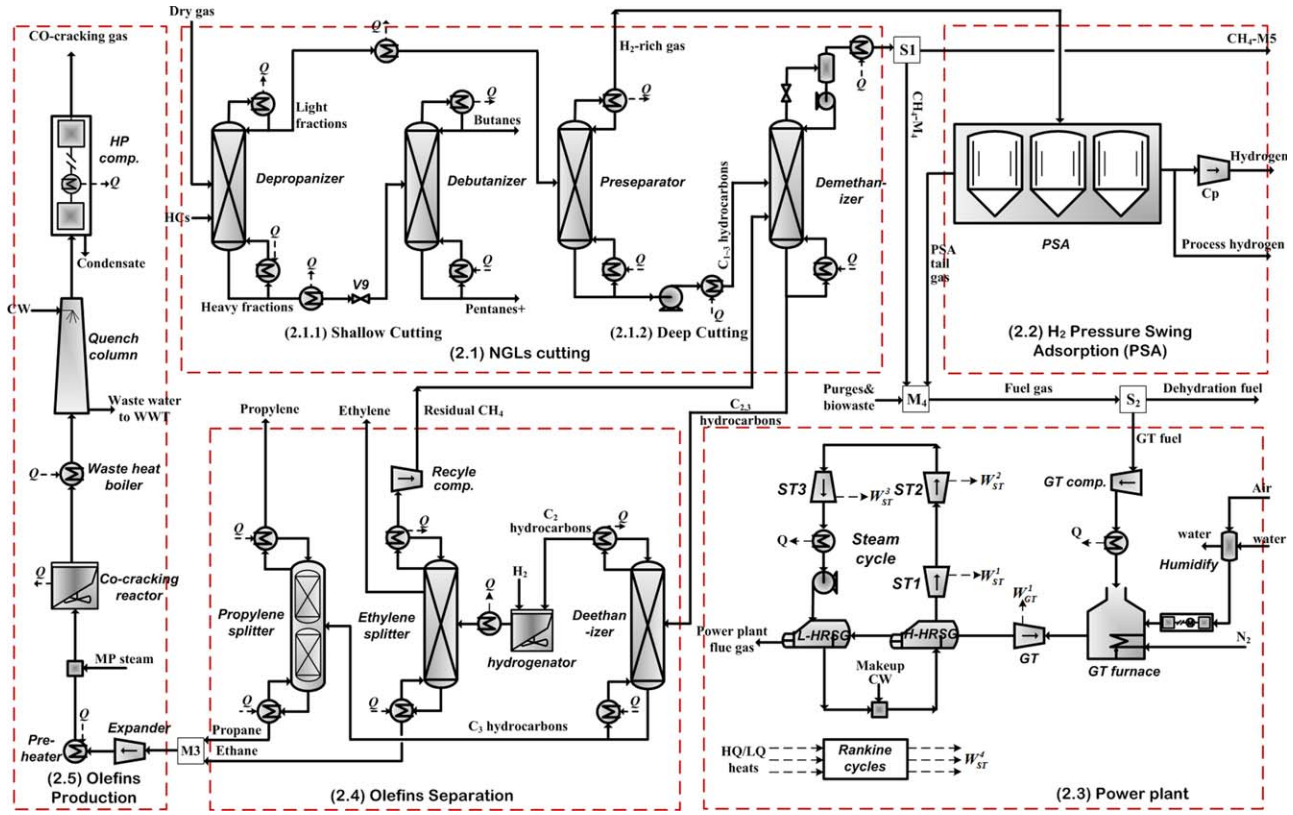

Figure 3. Flow sheet of the gas-to-chemicals area.

(2.1) NGLs cutting; (2.2) H_2 PSA; (2.3) power plant; (2.4) olefins separation and (2.5) olefins production. [Color figure can be viewed in the online issue, which is available at wileyonlinelibrary.com.]

Empirically, the heavier fractions including butanes and natural gasoline are first extracted by a shallow cutting train (depropanizer and debutanizer). The light fractions from the top of depropanizer are cooled down to −50°C and are then sent to a deep cutting train to remove both H_2-rich gas and methane. Considering the low boiling points of methane and hydrogen, a preseparator is used to separate about 98% of the nonhydrocarbons from the C_{1-3} hydrocarbons. As a result, the H_2-rich gas contains the following components: 70.0 mol % H_2, 8.0 mol % CO, 7.0 mol % N_2, and 15.0 mol % CH_4. The bottom liquid from the preseparator is pumped to a demethanizer, designed to recover about 94.2% of ethane and 99.2% of methane from the incoming streams. For the purpose of enhancing ethane recovery, the demethanizer is modeled as a reboiled absorber where the top stream is cooled down and throttled to −130°C, then is sent to a K.O. drum where the overhead methane vapor (roughly 95 mol % of CH_4) is finally sent to the OCM process, while the bottom liquid containing about 80 mol % of C_{2+} hydrocarbons is pumped to the first stage of demethanizer.

H_2 PSA. In the next step, the H_2-rich gas is processed in a common PSA system for the recovery of hydrogen, see Figure (2.2). The PSA block is modeled as a component separator on the basis that PSA recovery and purity are not sensitive to changes in the composition and pressure of the inlet stream. Specifically, the PSA block is designed to recover 85.0% of the H_2 with 99.5 mol % purity, as given by Eqs. 6 and 7. Hydrogen exits the PSA block at 20 bar, and roughly 15% of the hydrogen is used as process hydrogen to hydrogenate sulfur dioxide and acetylene. The pressure of the final hydrogen product is increased to 60 bar, a pressure suited for long-range pipeline transport. Moreover, the remaining H_2 and impurities including the PSA tail gas are discharged at 1.5 bar and used as combustion fuel. The work consumption in PSA block is given by Eq. 8

$$\mathrm{MF}_{\mathrm{H_2,out}} = \frac{85.0\%\mathrm{mf}_{\mathrm{H_2}} \cdot \mathrm{MF}_{\mathrm{H_2,in}}}{0.995} \tag{6}$$

$$\mathrm{mf}_{j,\mathrm{out}} = (1-99.5\%)\frac{\mathrm{mf}_{j,\mathrm{in}}}{\sum \mathrm{mf}_{j,\mathrm{in}}} \; j=\{\mathrm{CO_2, CO, N_2, Ar, CH_4}\} \tag{7}$$

$$W_{\mathrm{PSA}} = 158 N_{\mathrm{s}} \cdot \mathrm{mf}_{\mathrm{in}} \cdot \left[\left(P_{\mathrm{PSA,out}}/P_{\mathrm{PSA,in}}\right)^{0.286/N_{\mathrm{s}}} - 1\right] \tag{8}$$

where $\mathrm{MF}_{\mathrm{H_2,out}}and\mathrm{MF}_{\mathrm{H_2,in}}$are the molar flow rates (kmol/hr) of H_2 and the feed stream, respectively; $\mathrm{mf}_{j,\mathrm{out}}$ and $\mathrm{mf}_{j,\mathrm{in}}$ are respectively the molar fractions of impurity species j in H_2 and the feed stream. P_{in} is the intake pressure, P_{out} is the delivery pressure, $\mathrm{mf}_{\mathrm{in}}$ represents the flow rate through the compressor, and $N_{\mathrm{s}} = 2$ is the number of stages of compression.[31]

Power Plant. As shown in Figure 3 (2.3), the power plant includes GTs, steam turbines (STs), heat recovery steam generators (HRSGs), and steam cycle sections. To satisfy the requirements of GT operation, both GT fuel and air are compressed to 16.2 bar. Note that the incoming air is humidified to augment the efficiency and power output of the GTs section. The GT furnace and the GTs convert the chemical energy in the supplied GT fuel into shaft work. We note that, a certain amount of pressurized N_2 (at 16.2 bar) from the ASU is also injected to dilute the GT fuel to lower the LHV of syngas fuel to 4.30 MJ/Nm^3 and to reduce the

Table 2. Column Design Specifications and Parameters

Item	Operating Condition		Product		Key Component Recovery
	Temperature (°C)	Pressure (bar)	Top	Bottom	Rate (mol %)
AGR absorber	[41.8, 50.7]	[29.2, 29.4]	Sweet gas	Rich DEA	H_2S: 99.9, CO_2 99.7
AGR stripper	[41.8, 50.7]	[29.2, 29.4]	Acid gas/OCM-CO_2	Lean DEA	DEA: 99.9
TEG contactor	[32.5, 33.2]	[29.0, 29.2]	Dry gas	Rich TEG	H_2O: 99.9
TEG still	[80.9, 185.0]	[29.2, 29.4]	Water gas	–	TEG: 99.9
Surge tank	[167.3, 177.5]	[1.1, 1.2]	–	Lean TEG	–
AGE absorber	[30.3, 41.5]	[0.55, 0.65]	CO_2 slip	Rich MDEA	CO_2: 82.4
AGE costripper	[58.0, 117.0]	[1.5, 1.6]	Enriched gas	Lean MDEA	MDEA: 99
SCOT absorber	[30.0, 38.6]	[1.0, 1.2]	Sweet gas	Rich MDEA	H2S: 99
Depropanizer	[−46.4, 141.9]	[26.0, 26. 5]	Light fraction	Heavy fraction	Propane:97.7
Debutanizer	[7.0, 7.5]	[29.2, 29.4]	Butanes	Natural gasoline	Butanes:98.0
Preseparator	[−90.5, −149.5]	[25.0, 26.0]	H_2-rich gas	C_{1-3} HCs[a]	Methane:98.0
Deethanizer	[−7.7, 70.0]	[27.3, 27.9]	C_2 HCs	C_3 HCs	Ethane:99.8
Demethanizer	[8.0, −83.1]	[30.0, 33.0]	Methane	$C_{2,3+}$ HCs	Methane:99.2
Ethylene splitter	[−6.7, −70.0]	[19.5, 20.5]	Residual CH_4	Ethane	Ethylene:99.9
Propylene splitter	[44.9, 58.6]	[19.3, 20.7]	Propylene	Propane	Ethane:95.0
Ethylene splitter[b]	[−8.5, −25.0]	[26.2, 27.0]	Light by-product	Heavy by-product	Ethylene:99.9
Ethylene stripper[b]	[−5.3, −20.7]	[25.2, 26.0]	Stripping gas	Bioethylene	–

[a]Hydrocarbons.
[b]In bioethanol to ethylene area.

NO_x formation.[35] Using two HRSGs in series, the flue gas from the GT section exchanges heat with process steam in the steam cycle to provide the steam needed in the STs, which also produce work. The steam cycle in this model has three pressure levels: high pressure (HP, 125 bar, 550°C), medium pressure (MP, 60 bar, 380°C), and low pressure (LP 29 bar, 290°C). Additionally, two predefined Rankine cycles with heat engines are designed to collect waste heat from across the system to generate steam. A more detailed design of the Rankine cycle is outside the scope of this article. The work produced from the GTs, STs, and Rankine cycles is converted to electricity through generators.

Olefins Separation. The olefins separation process includes four major equipment units: a deethanizer,a hydrogenator, an ethylene splitter, and a propylene splitter [Figure 3 (2.4)]. The deethanizer first recovers C_2 hydrocarbons from the liquid stream from the bottom of the demethanizer. The deethanizer top stream first passes through the hydrogenation reactor, where a small amount of acetylene (0.02–0.10 mol %) is completely removed according to reactions (9) and (10). Afterward, the reactor effluent is cooled and sent to the ethylene splitter. Similarly to the demethanizer, the ethylene splitter operates at low temperatures, ranging from −10 to −70°C, to separate the feed stream into three products. The ethylene splitter top product, which contains about 75 mol % methane and 25 mol % ethylene, is compressed and recycled to the demethanizer to boost the ethylene recovery rate. The side-draw product with 99.9 mol % of polymer grade ethylene is a marketable chemical product. The third product leaving from the bottom of the splitter contains more than 90 wt % ethane and is fed to the downstream olefins production process as the main feedstock. The last distillation process, a propylene splitter, integrates two subdistillation units that purify the propylene product to chemical grade standard (96.0 mol %). The detailed operating parameters used in the column design are listed in Table 2.

$$C_2H_2 + H_2 \rightarrow C_2H_4 \quad (9)$$

$$C_2H_2 + 2H_2 \rightarrow C_2H_6 \quad (10)$$

Olefins Production. Minimizing the number of reactors in a modern large steam cracking plant will help reduce the project capital cost for the given installed capacity.[32] Thus, it is important to maintain high feedstock flexibility in the design of a cracking plant. Feedstock flexibility refers to the capability to crack a range of raw materials, and incorporate the cocracking or hybrid cracking processes. This model considers the ethane and propane to be thermally cracked in a single reactor, as depicted in Figure 3 (2.5). The performance of cocracking reactor will be influenced by the operating conditions (see Table 3), which are controlled by an expander and a preheater. The stream is then diluted with MP steam (MPS/ethane = 0.3 in mass basis) in a mixer. After that, it goes into a convection/radiation cracking reactor, where ethane molecules are broken up to generate ethylene, propylene, hydrogen, methane, acetylene, and so forth. Several molecular reaction schemes have been proposed for

Table 3. Decision Variables Used in This Simulation-Optimization Work

Variable	Notation	Unit	Range	Note
Distribution ratio at point S_1	X_{s1}	mol/mol	[0,0.20]	Structural variables, CH_4-M_4/S_1 inlet
Distribution ratio at points S_2	X_{s2}	mol/mol	[0,0.8]	Structural variables, dehydration fuel/S_2 inlet
OCM temperature	T_{OCM}	°C	[800,900]	Operating variables
OCM pressure	P_{OCM}	bar	[1.1,2.2]	Operating variables
OCM O_2 feed	R_{O_2}	mol/mol	[0.20,0.80]	Operating variables
Cocracking temperature	T_{ccr}	°C	[700,800]	Operating variables
Cocracking Pressure	P_{ccr}	bar	[3.0,3.5]	Operating variables

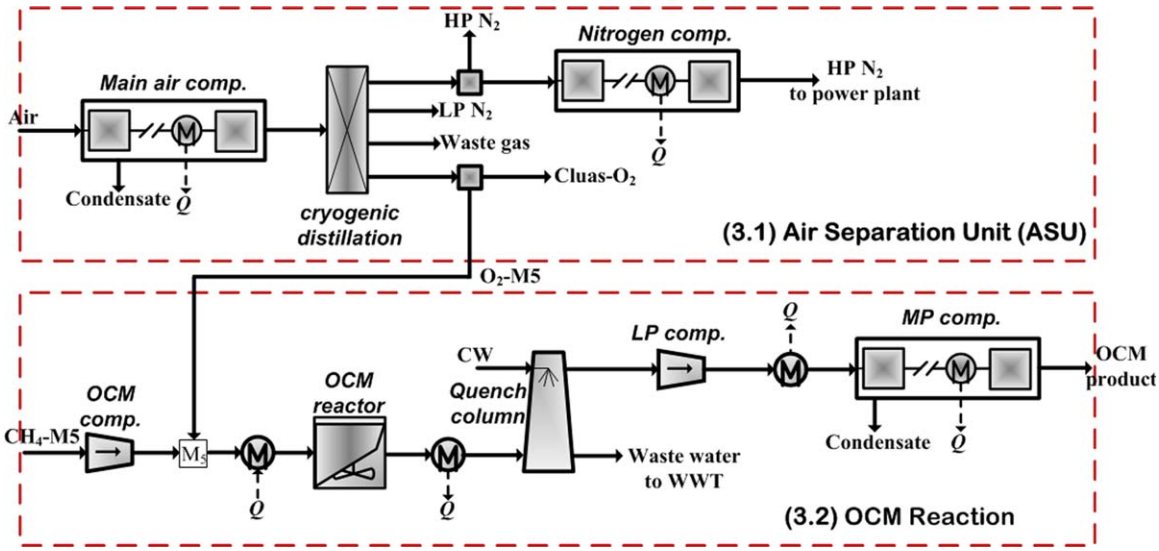

Figure 4. Flow sheet of methane to ethylene area.

[Color figure can be viewed in the online issue, which is available at wileyonlinelibrary.com.]

the pyrolysis of ethane. Typically, the cracker reactor is a plug flow reactor which can be approximated in HYSYS through a series of continuous stirred-tank reactors (CSTRs) with simple rate kinetic equations according to Forment's 10 independent reactions scheme,[42,43] as given by R(1)–(10) in Table B1 in Appendix B. The comparison of industrial and modeling outputs for this kinetic model can also be found in this table. This comparison reveals that the model performs better for the cracking process. The produced cocracking gas is a mixture of C_2H_4, H_2, C_2H_6, CH_4, and so forth, which can be further processed. It is first gas stream is cooled to 35°C by exchanging heat with a waste heat boiler and a quench column in series. Next, this cooled stream flows into a three-stage compression system, and is finally sent to the dehydration unit.

Methane-to-ethylene area

Air can be directly used as an oxidant source and nitrogen is used as a diluent in the reactor section to reduce the possibility of hot spot formation. However, the low O_2 concentration in the reaction side causes long mixing times and a rather slow reaction rates, and inevitably increases the complexity of product separation.[12,44] Hence, in this work O_2 is used to oxidize CH_4 in OCM reactor. An ASU is used to recover O_2 from the incoming air by cryogenic distillation. Figure 4 shows the process flow diagram of the methane-to-ethylene area. Air is first compressed to 13.1 bar via a four-stage main air compressor with interstage coolers and K.O. drums. The dehydrated air is sent to a complex cryogenic distillation system, modeled as a component separator and assumed to have the following specifications: O_2 is recovered at 10.0 bar and 32.2°C with component recovery rates of $O_2-0.94$, $N_2-0.005$, and Ar-0.704; HP N_2 is recovered at 12.6 bar and 10.0°C with component recovery rates of $O_2-0.002$, $N_2-0.119$, and Ar-0.024; LP N_2 is recovered at 3.9 bar and 32.2°C with component recovery rates of $O_2-0.015$, $N_2-0.736$, and Ar-0.146; and the remaining gases are considered waste gases and discharged at 1.1 bar. A small amount of O_2 (0.5–2.0%) is used for the Claus process. Meanwhile, about 50–90% of HP N_2 is split, compressed, and sent to the GT furnace in the power plant. The remaining the HP N_2 is expanded through turbines to recover energy and then vented to the atmosphere with the LP N_2. The total ASU power requirement (W_{ASU}) is based on the specified purity of O_2 which may be estimated according to the following correlation[35]

$$W_{ASU}=W_{aircomp}\times\beta$$

$$\beta=\begin{cases}5.4992\times C_{O_2}, C_{O_2}\in(95\%,97.5\%)\\ 8.295\times10^2/(100-C_{O_2}^{1.136})+0.988618, C_{O_2}\in(97\%,99.5\%)\end{cases} \quad (11)$$

where $W_{aircomp}$ is the net power consumption of the main air compressor (MWh), and C_{O_2} is the O_2 molar purity (%).

The CH_4 stream (CH_4-M_5) split from point S_1 is compressed to OCM reaction pressures ranging from 1.1 to 2.2 bar and then mixed with O_2 at point M_5. The mixture is heated to 600°C and then sent to an OCM reactor. Though different OCM reaction systems have been investigated both theoretically and experientially, there are very few detailed macrokinetic models or pilot tests. In this model, one of the most well-known fixed-bed OCM reactor with La_2/CaO catalyst is used.[45] The fixed-bed OCM reactor represents a simple structure and includes only one catalyst bed. All the reactants consisting of methane and oxygen are cofed in the catalyst bed, where all the reactions take place. The OCM reactor is modeled as an isothermal CSTR with an exterior cooling wall operating at 800–900°C. This model consists of three primary and seven consecutive reactions, listed in Table B2 in Appendix B. In this work, it is assumed that an industrial scale OCM process for about 75,000 ton ethylene/year capacity is adapted. The total OCM reactor is determined by the reasonable and verifiable conversion rate of methane, shown in Figure 5. The OCM effluent exiting from reactor is cooled to 100°C and then quenched to 35°C by cooling water. Next, the dehydrated OCM product is compressed to 5.0 bar by an LP compressor followed by a two-stage MP compressor. Finally, the OCM product at a pressure of 30.0 bar goes to gas sweetening unit in the gas treatment area for CO_2 removal.

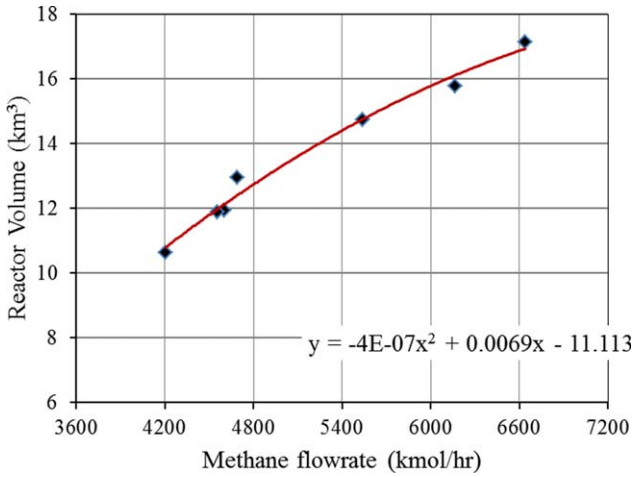

Figure 5. The relationship between methane conversion rate and CSTR volume.

The CSTR is operating at 801°C, 3.3 bar and O_2/CH_4 = 0.65 on molar basis.[13] [Color figure can be viewed in the online issue, which is available at wileyonlinelibrary.com.]

Bioethanol-to-ethylene area

Figure 6 shows the process flow diagram of bioethanol-to-ethylene area. Before entering the dehydrator, the corn-derived ethanol (95 wt %) is pumped and vaporized at 12.0 bar and 450°C. In practices, superheated steam is also directly injected into the dehydrator at a 1:1 weight proportion to the feed, to achieve a high conversion and selectivity. In the dehydrator, the reactants are evaporated in the first part of the reactor packed with the inert material. Then, reactants vaporized are supplied to the catalyst bed and converted to ethylene and various by-products. In this work, the dehydrator is modeled as an adiabatic, stoichiometric reactor operating at 11.4 bar, and the corresponding reactions[46] with their selectivities are given by Eqs. 12–19. As mentioned in Introduction, BD is a strongly endothermic reaction which is fueled by the heat from dehydration fuel combustion. The reactor effluent is cooled in the quench column. Consequently, water present in the effluent is condensed. The pressure of the quench column overhead is increased to 27 bar in an LP compressor followed by a two-stage MP compressor. Next, a trace amount of CO_2 and water are rejected from this stream in a caustic column and a molecular sieve dryer. Finally, the dehydrated stream containing 98.7 mol % of ethylene is precooled to −20°C and further purified in a cryogenic ethylene splitter, followed by an ethylene stripper.[46] The overhead (light by-product) from the partial condenser, together with the bottom stream (heavy by-product), are sent to point M_4 and used as process fuel. The overhead of the stripper is recycled to the distillation column to minimize ethylene loss. Finally, the bioethylene product meets the following polymer grade standard: $C_2H_4 >$ 99.9 mol %, CO < 5 ppm, CO_2 < 10 ppm, and (C_2H_6 + C_2H_6) < 0.15 mol %[47]

$$C_2H_5OH \rightarrow C_2H_4 + H_2O \quad 98.8\% \tag{12}$$

$$2C_2H_5OH \rightarrow (C_2H_5)_2O + H_2O \quad 0.052\% \tag{13}$$

$$C_2H_5OH \rightarrow C_2H_4O + H_2 \quad 0.2\% \tag{14}$$

$$2C_2H_5OH + H_2 \rightarrow 2n\text{-}C_3H_6 + 2H_2O \quad 0.27\% \tag{15}$$

$$3C_2H_5OH \rightarrow 2n\text{-}C_3H_6 + 3H_2O \quad 0.06\% \tag{16}$$

$$2C_2H_5OH \rightarrow n\text{-}C_4H_8 + 2H_2O \quad 0.5\% \tag{17}$$

$$C_2H_5OH \rightarrow CO + CH_4 + H_2 \quad 0.007\% \tag{18}$$

$$C_2H_5OH + H_2O \rightarrow 2CO_2 + CH_4 + H_2 \quad 0.11\% \tag{19}$$

Simulation-Based Optimization

General methodology and framework

Figure 7 shows the framework of the simulation-optimization method, which performs LCO of the process modeled in Aspen HYSYS, we develop a simulation-optimization method based on the evolutionary NSGA-II algorithm.[48] An energy integration model is also fluidly

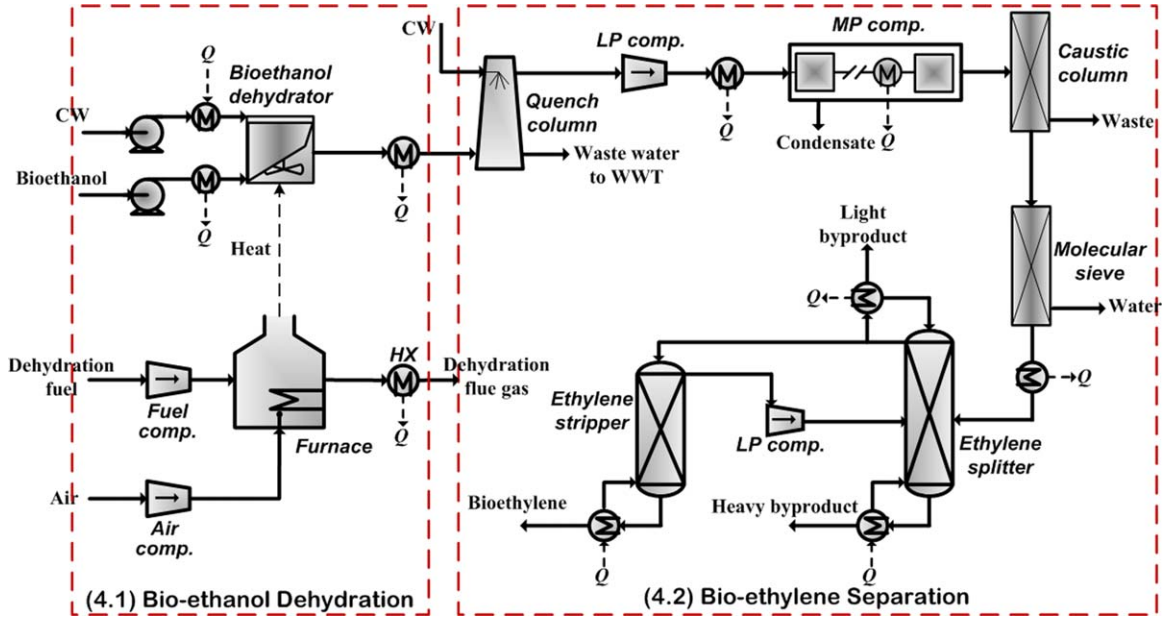

Figure 6. Flow sheet of bioethanol to ethylene area.

[Color figure can be viewed in the online issue, which is available at wileyonlinelibrary.com.]

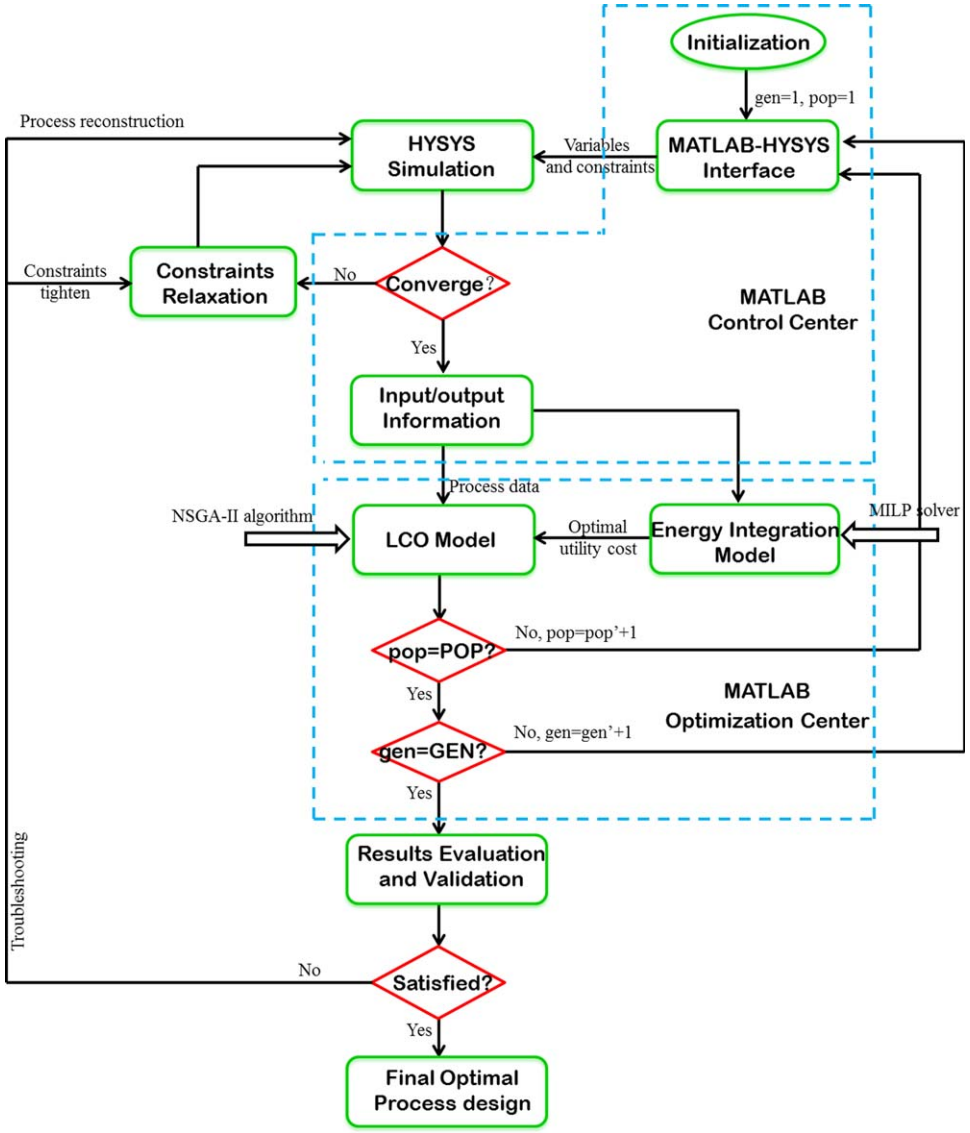

Figure 7. Schematic diagram of the simulation-optimization framework.

[Color figure can be viewed in the online issue, which is available at wileyonlinelibrary.com.]

nested using an MILP. First, in the MATLAB control center, the initial chromosomes (population = 1, individual = 1) that contain decision variables are randomly generated in the selected ranges listed in Table 3. These decision variables with constraints are supplied to the process simulator via a MATLAB-HYSYS interface. Then, the MATLAB control center will automatically check the convergence of the HYSYS simulation. If infeasible, we can relax the corresponding constraints on the complex equations of simulation model. Note that, the strategies for better convergence and computation time reduction are systematically described in Appendix B. Otherwise, process operating variables are temporarily fixed, and the input/output information taken from simulation results can be collected, mapped, and prepared for the next MATLAB optimization center where two subproblems are successively performed. In the first subproblem, the utility-related data including heat, power, temperature, refrigerant, and cooling water for each process area are given to the energy integration model. Then, this model is optimized by an MILP solver to determine the minimum total cost of hot/cold/power utility. The resulting optimal utility cost (C_{uti}) from the energy integration model, combined with the process data (feedstocks, products, solvents, cost, and emissions) is passed to a multiobjective LCO model.[49] The NSGA-II algorithm[48] is used to obtain the Pareto-optimal sets of techno-economic and environmental impact objectives included in the LCO model through the reproduction of population and individuals. The proposed framework is finally terminated after a predefined generation number is reached. Based on the Darwinian principle of survival of the fittest, NSGA-II uses a fast nondominated sorting approach to solve constrained multiobjective problems efficiently. The parameters used in the NSGA-II algorithm include: population size (POP)-30, maximum generation (GEN)-100, crossover probability-1.2 (intermediate), and mutation probability-0.5 (Gaussian). Finally, the result of the optimal process design is guaranteed by evaluating and validating the results. If the validation results are not satisfied, either the relaxed constraints should be tightened using rigorous simulation, or the whole/local process model should be reconstructed with Aspen HYSYS.

Table 4. Parameters and Assumptions Used for Economic and Environmental Impact Evaluation (2012 USD)

Items	Base Values	Uncertain	Items	Base Values	Uncertain
Shale gas	$ 5.52/GJ	U[a] (3.50,7.50)	Butanes	$ 1.60/gal	U (1.0,2.2)
Bioethanol	$ 2.23/gallon	U (1.80,2.80)	Natural gasoline	$ 2.20/gal	U (1.5,3.5)
Ethane	$ 0.50/gal	U (0.2,0.8)	Hydrogen	$ 1.76/kg	U (1.3,2.2)
Ethylene	$ 1200/ton	U (900,1500)	Propylene	$ 1340/ton	U (800,1800)
R1[b] (0 to −20°C)	$ 2.65/GJ	U (2.00,3.50)	Sulfur	$ 200/ton	U (100,300)
R2 (−20 to −50°C)	$ 4.65/GJ	U (4.00,5.60)	Electricity	$ 0.07/kWh	U (0.04,0.1)
R3(−50 to −80°C)	$ 6.64/GJ	U (6.00,5.60)	LP steam	$ 3.11/GJ	U (2.50,4.00)
R4 (−80 to −100°C)	$ 7.96/GJ	U (7.00,8.90)	HP steam	$ 6.68/GJ	U (5.50, 8.00)
R5 (−100 to −130°C)	$ 9.96/GJ	U (9.00,10.9)	Water	$ 0.03/ton	U (0.01,0.06)
R6 (−130 to −160°C)	$ 11.94/GJ	U (11.0,12.9)	Solvent	$ 2700/ton	U (2200,3200)
IR	0.03	Coproduct	Raw Material	GWP	Reference
R	15%	Hydrogen	Natural gas	11.15 kg CO_2-eq/kg	GREET[50]
R_{tax}	30%	Propylene	Fossil	1.98 kg CO_2-eq/kg	Ecoinvent[51]
T_{ls}	20 years	Butanes	Fossil	0.96 kg CO_2-eq/kg	GREET[50]
T_{dp}	6 years	Natural gasoline	Fossil	1.52 kg CO_2-eq/kg	Ecoinvent[51]
AT	8000 h/year	Sulfur	Sulfide ores	0.43 kg CO_2-eq/kg	Ecoinvent[51]
ICF/BOPF	32%/20%	Electricity	Fossil	89.4 kg CO_2-eq/GJ	IPCC[52]

[a]Uniform distribution.
[b]Refrigerant.

Energy integration model

The objective of the energy integration model is to minimize the external utilities supply (power, HP/MP/LP steams, cooling water, and refrigerant) by exchanging heat between the available energy sources and sinks, subject to a minimum temperature of approach for heat transfer. In addition, the waste heat streams can either provide steam or generate power using a heat exchange/power recovery (HEP) network that consists of heat exchangers, water boilers, heat engines, and heat pumps.[37] In this work, we allow for simultaneous power generation from the waste heat using a set of predefined Rankine cycles.[33] The objective function, as presented in Eq. 20, is to minimize the total cost of hot/cold/power utility necessary to accomplish the desired thermal task. The parameters used in energy integration are listed in Table 1

$$SP1\ \min C_{\text{uti}} = \sum_{i^{\text{H}} \in \text{UH}_k} C^{\text{U}}_{i^{\text{H}}} Q^{\text{U}}_{i^{\text{H}}} + \sum_{i^{\text{C}} \in \text{UC}_k} C^{\text{U}}_{i^{\text{C}}} Q^{\text{U}}_{i^{\text{C}}} + \sum_{j \in \text{EP}_k} W_{\text{con},j} - C_{\text{ele}} \sum_{i^{\text{H}} \in \text{UH}_k} W_{\text{HEP},k} \tag{20}$$

$$\text{s.t.} \quad R_k - R_{k-1} = [F^{\text{H}}_{Cp,k}\alpha_k + (F_{Cp,k})_{\text{H},k}\delta_k](T^{\text{H}}_k - T^{\text{H}}_{k+1}) - [F^{\text{C}}_{Cp,k} + (F_{Cp,k})_{\text{H},k}\chi_k](T^{\text{C}}_k - T^{\text{C}}_{k+1}) \tag{21}$$

$$W_{\text{HEP},k} = F^{\text{H}}_{Cp,k}(1-\alpha_k)(T^{\text{H}}_k - T^{\text{H}}_{k+1})\eta_k \tag{22}$$

$$\begin{cases} R_k \geq 0; R_1 = R_K = 0; \forall k \in [1, K-1] \\ \alpha_i \in [0,1]; \forall k \in [1, K-1] \\ Q^{\text{U}}_{i^{\text{H}}} \geq 0; Q^{\text{U}}_{i^{\text{C}}} \geq 0; W_{\text{con},j} \geq 0 \end{cases} \tag{23}$$

$$\delta_k = \begin{cases} 1; \text{if } T^{\text{H}}_k > T^{\text{H}}_{\text{out}} - \Delta T_{\min,\text{H}} \\ 0; \text{if } T^{\text{H}}_k \leq T^{\text{C}}_{\text{out}} - \Delta T_{\min,\text{H}} \end{cases} \forall i \in [1, K] \tag{24}$$

$$\chi_k = \begin{cases} 1; \text{if } T^{\text{C}}_k \leq T^{\text{C}}_{\text{out}} + \Delta T_{\min,\text{C}} \\ 0; \text{if } T^{\text{C}}_k > T^{\text{C}}_{\text{out}} + \Delta T_{\min,\text{C}} \end{cases} \forall k \in [1, K] \tag{25}$$

The complete nomenclature is provided at the end of this article. $C^{\text{U}}_{i^{\text{H}}}$ and $C^{\text{U}}_{i^{\text{C}}}$ denote the unit cost of the hot utility i^{H} and cold utility i^{C}, respectively, with $i^{\text{H}} \in$ {hot water, HP/MP/LP steams}hot water, HP/MP/LP streams and $i^{\text{C}} \in$ {cooling water, refrigerants}; $Q^{\text{U}}_{i^{\text{H}}}$ and $Q^{\text{U}}_{i^{\text{C}}}$, respectively, denote the heat load of the hot utility stream i^{H} and cold utility stream i^{C}; $W_{\text{con},j}$ represents the power needed for equipment (EP) j and $W_{\text{HEP},k}$ is the work generated from the HEP network in temperature interval k. Equation 21 is the transshipment model where a fraction α_k of the available heat comes from the hot composite curve in interval k. Meanwhile, the respective complementary fraction $(1-\alpha_k)$ is used in the HEP network, and η_k is the overall energy efficiency of Rankine cycle in interval k, as shown in Eq. 22. The relevant constraints can be found in Eqs. 14–16. Due to the relatively small size, the MILP model is formulated and then solved using the *Intlinprog* function in MATLAB Toolbox to obtain the optimal HEP networks and minimum utility cost (C_{uti}). In the MILP subproblem, only the minimum utility cost is targeted for the given process streams. The inlet/outlet temperatures, utilities costs, and parameters details are listed in Tables 1 and 4. The capital cost for energy integration is addressed in the next economic objective function.

LCO model

The LCO approach integrates a multiobjective optimization scheme and a life cycle analysis method.[53] It is used to provide further insights into the process design problem and improve the inherent trade-offs between the economic and environmental performances in the context of sustainability.[54–59] In the LCO model, the techno-economic objective function considers the minimization of the NPV indicator which measures the sum of a series of discounted cash flows, both incoming and outgoing, over the entire lifetime of the project. The incoming cash flows of the process include sales revenue (Rev) from olefins, hydrogen, and heavy NGLs. The outgoing cash flows refer to a one-time investment, total plant capital cost (TPC), and total annual cost (TAC) that includes fuel cost (AFC), nonfuel operating and maintenance cost (AOC), as well as federal and state taxes. The products (i.e., ethylene and propylene) are assumed to be sold from the plant gate and do not include the transportation cost to end-users. For expenses, the break-even gas price (BEGP) of raw shale gas from wellhead varies from well to well, which is assumed to be $5.52 per GJ on average based on point-forward calculations.[60] The compressed CO_2 is transported via pipeline with an average length of 250 km. The

operating cost and geological storage cost are based on an IPCC study.[61]

All investments in basic equipment is predicted by the Aspen Process Economic Analyzer,[62] or taken from several literature sources.[25,46,63–66] The Chemical Engineering Plant Cost Index[50] is used to convert the capital cost numbers to 2012 dollars. The total installed cost (TIC) of an equipment is calculated by multiplying the equipment purchase cost by the installation factor, IF. As given by Eq. 26, the TIC along with the balance of plant (BOP), and the indirect cost (IC) gives an estimate of the TPC required for the project. In this model, the BOP includes the capital costs associated with warehouse, site development, and piping network and is estimated to 20% of the TIC. In addition, the IC including engineering, startup, spares, royalties, and contingencies is estimated to 32% of the TDC. Detailed capital cost parameters used in this calculation are given in Supporting Information Table S1

$$\begin{aligned}\mathrm{TPC}&=\mathrm{TDC}+\mathrm{IC}=\mathrm{TIC}+\mathrm{BOP}+\mathrm{IC}\\&=(1+\mathrm{bop}+\mathrm{ic})\cdot[\mathrm{IF}\cdot C_0\cdot(S_r/S_0)^{\mathrm{sf}}]\end{aligned}\tag{26}$$

where bop, ic, C_0, S_r, S_0, and sf are the balance of plant factor, indirect cost factor, basic equipment purchase cost, actual capacity, base capacity, and cost scaling factor, respectively. Assuming an operating capacity of 8000 h/year, the TPC can be translated to a levelized cost to compare with the annual fuel costs (AFC) and annual operating costs (AOC) for the process using a capital recovery factor (CRF). The CRF is determined as a function of the interest rate (IR) and depreciation time of the project (T_{dp}). For NPV calculation, we considered a plant life span of 20 years ($T_{\mathrm{ls}}=20$), and the tax rate (R_{tax}) and discounted annual rate (r) to be 15 and 30%, respectively. In addition, the revenue of this process, Rev, comes from selling ethylene, propylene, butanes, natural gasoline, hydrogen, and sulfur at market prices listed in Table 4. The aforementioned indicators and parameters are given below

$$\mathrm{TAC}=\mathrm{TPC}\times\mathrm{CRF}+\mathrm{AOC}+\mathrm{AFC}\tag{27}$$

$$\mathrm{CRF}=\mathrm{IR}(\mathrm{IR}+1)^{T_{\mathrm{dp}}}/[(1+\mathrm{IR})^{T_{\mathrm{dp}}}-1]\tag{28}$$

$$\mathrm{NPV}=-\mathrm{TPC}+\sum_{t\in T_{\mathrm{ls}}}\frac{(\mathrm{Rev}-\mathrm{TAC})(1-R_{\mathrm{tax}})}{(1+r)^t}\tag{29}$$

GWP is a relative measure of how much radiated heat is trapped by GHG emissions in the atmosphere and is calculated over a specific time interval. The GWP calculations considered in this model that focus on the global warming effects caused by CO_2, CH_4, SO_2, and NO_x. Note that, a cradle-to-gate boundary of the LCO analysis is used due to the process involves the production of chemicals (not liquid/gas fuels). In addition, our approach focuses mainly on reducing the environmental impact of the manufacturing stage. As pointed out by a number of existing publications,[51,52,67,68] the downstream processes such as secondary processing, product use, and disposal can be neglected. The GHG emissions of the process are calculated from three stages below.

Stage (1) involves the emissions during the preparation of feedstock and utility (PFU). The PFU involves shale gas, bioethanol, electricity, refrigerant, and steam. Among them, corn-derived bioethanol is purchased from market, and the plant-level GHG emissions are equal to 0.042 kg CO_2-eq per GJ bioethanol.[69,70] The GHG emissions for shale gas preparation will be discussed later. The GHG emissions associated with ethanol transportation, plant equipment production and installation, and plant construction are not considered.

Stage (2) involves plant-wide direct CO_2 venting throughout plant operation. The waste streams include the flue gases emitting from the incinerator in the sulfur recovery unit, from the GT furnace in the power plant, and from the dehydration furnace in the BD unit.

Stage (3) concerns the GHG emissions associated with CO_2 sequestration. The major parameters related to this stage are given below. The CO_2 leakage rate and recompression power consumption for pipeline transportation are assumed to be 0.026%/(million meter) and 0.011 kWh/(1 km ton CO_2), respectively.[71] The power requirement for CO_2 deep saline injection is assumed to be 6.68 kW/ton CO_2.[71]

As mentioned in Introduction, methane leakage is the most important consideration for the environmental impacts of shale gas production, but existing studies do not reach an agreement in terms of range of data employed. The data used in this work regarding methane emission factors ($\gamma_{\mathrm{SG,CH_4}}$, methane leakage/natural gas produced, v/v%) are taken from several well-cited articles.[21,72,73] Given the uncertainty in the data used, the GWP indicator is evaluated in two scenarios as follows.

1. Low carbon shale gas (LCSG), where shale gas is considered as a low carbon fuel and the emissions factor is 1.19% according to the GREET model reported by Argonne National Laboratory.[73]

2. High carbon shale gas (HCSG), where Howarth's viewpoint[21] is adopted, and 3.30% of the lifetime production of gas from wells is emitted as methane. The GWP is calculated by Eq. 30 below

$$\begin{aligned}\mathrm{GWP}=\mathrm{AT}[&\sum_{b\in\mathrm{LCI}}\sum_{v\in\mathrm{WS}}\mathrm{MF}_v\mathrm{FR}_b\varphi_b\\&+\mathrm{MF}_{\mathrm{SG}}/\mathrm{mw}_{\mathrm{SG}}\varphi_{\mathrm{CH_4}}\gamma_{\mathrm{SG,CH_4}}/(1-\gamma_{\mathrm{SG,CH_4}})\\&+\sum_{l\in\mathrm{PFU}/\{\mathrm{SG}\}}\mathrm{MF}_l\varphi_{\mathrm{CO_2}}\theta_{l,\mathrm{CO_2}}-2\mathrm{MF}_{\mathrm{bio}}/\mathrm{mw}_{\mathrm{bio}}\mathrm{mw}_{\mathrm{CO_2}}\varphi_{\mathrm{CO_2}}]\end{aligned}\tag{30}$$

where AT is the annual operating time; MF represents the mass flow rate of the waste stream v and feedstock l; φ_b is the damage factor which accounts for the GWP associated with chemical b relative to that of CO_2, and $\mathrm{LCI}=\{CO_2,\ CH_4,\ SO_2,\ \text{and}\ NO_x\}$; $\theta_{l,\mathrm{CO_2}}$represents the equivalent amount of CO_2 emission associated with the production of l except the shale gas; mw and FR are molar weight and weight fractions, respectively. For the calculation of GWP for unit ethylene, the mass-based allocation method is used to handle coproducts. These data are updated from GREET[34] and Ecoinvent[36] databases and IPCC[74] report (Table 4).

To cover both the techno-economic and environmental impact targets and allow for a clear analysis of the results, two consistently aggregated performance indicators are simultaneously used as process optimization objectives, shown in Eq. 31. The techno-economic indicator, NPV, defined in Eq. 29, comprises all costs and profits directly linked to it (i.e., equipment, raw materials, products, and utilities). With regard to environmental impact analysis, the GWP defined in Eq. 30 is used as the indicator to assess the impact of the GHG emissions to the environment.

Table 5. Solution Comparison Between Two Scenarios for the Three Pareto Points

CUP Time (h)		NPV ($MM)		GWP (kton CO_2-eq/year)	
LCSG scenario	HCSG scenario	LCSG scenario	HCSG scenario	LCSG scenario	HCSG scenario
A_1: 105.1	A_2: 104.2	A_1: 1457	A_2: 1322	A_1: 211.2	A_2: 436.2
B_1: 101.5	B_2: 100.5	B_1: 1334	B_2: 1101	B_1: 177.2	B_2: 313.5
C_1: 92.5	C_2: 121.2	C_1: 585.1	C_2: 577.7	C_1: −154.6	C_2: 102.9
Decision variable in LCSG scenario			Decision variable in HCSG scenario		
($X_{S1}/X_{S2}/T_{OCM}/P_{OCM}/R_{O_2}/T_{ccr}/P_{ccr}$)			($X_{S1}/X_{S2}/T_{OCM}/P_{OCM}/R_{O_2}/T_{ccr}/P_{ccr}$)		
A_1: 0.0001/0.240/815.1/189.5/0.225/785.7/351.3			A_2: 0.0002/0.750/817.2/189.2/0.235/789.1/353.5		
B_1: 0.0017/0.542/810.1/180.4/0.237/767.5/340.1			B_2: 0.045/0.710/845.2/187.0/0.322/770.2/342.4		
C_1: 0.1870/0.795/825.0/139.2/0.295/750.2/335.0			C_2: 0.202/0.790/852.5/140.2/0.320/755.1/325.0		
GWP_{E2E} ($kgCO_2$-eq/kg ethylene)		MESP ($/ton ethylene)		Bioethanol/SG (mol/mol)	
LCSG scenario	HCSG scenario	LCSG scenario	HCSG scenario	LCSG scenario	HCSG scenario
A_1: 0.119	A_2: 0.804	A_1: 476.5	A_2: 712.2	A_1: 0.099	A_2: 0.319
B_1: −0.030	B_2: 0.360	B_1: 655.1	B_2: 877.2	B_1: 0.245	B_2: 0.576
C_1: −0.615	C_2: −0.115	C_1: 1070.6	C_2: 1075.8	C_1: 1.053	C_2: 1.092

$$SP2 \min \begin{cases} f_1 = -\text{NPV} \\ f_2 = \text{GWP} \end{cases}$$
$$\text{s.t. mass/energybalanceconstraintsintheHYSYS}$$
$$\text{unit specifications and parametersintheHYSYS} \quad (31)$$
$$\text{decision variables and constraintsin Table 3}$$
$$\text{economicevalutaionconstraintsEqs.26}-28$$

The sequential simulation-optimization approach adapted in this work is of a heuristic class. Therefore, it cannot guarantee that a global optimum is found. The best solution's distance from the true optimum would depend on the search starting points, the feasible regions, the number of steps, the number of iterations, and so forth.[75,76] Note that, the Aspen HYSYS contains complex physical/chemical properties and nonlinear thermodynamic equations. As a result, the presented search may be difficult to converge when the selected variables have coarse search ranges. However, too narrow range would result in a large computational scale, also excluding the true optimum far from the solution due to iteration numbers and time constraints.[75] To overcome these challenges, we first propose a systematic relaxation strategy in Appendix C to guarantee a feasible solution and reduce the computational time. Additionally, to evaluate the trade-off between the economic and environmental performances, thereby obtaining the optimal process design, several parameters can be tuned at selected ranges. The decision variables for the process consist of two categories of parameters: structural variables, which refer to the distribution ratios at points S_1 and S_2, and operating variables, which include the key operating conditions of the major reactions (OCM and cocracking). Table 3 lists the seven selected decision variables with constrains for the optimization of the proposed process.

Results and Discussion

The simulation-optimization model is realized by combining MATLAB R2010a and Aspen HYSYS V7.2. All computational studies were performed on a DELL OPTIPLEX 790 desktop with an Intel(R) Core(TM) i5–2400 CPU @3.10GHz and 4 GB RAM, using Windows 7 64 bit operating system. Calculation times are given in Table 5.

Pareto-optimal designs and solution analysis

Figures 8a, b show the Pareto curves for both HCSG and LCSG scenarios. In this figure, the vertical coordinate is the GWP in kton CO_2-eq/year, and the horizontal coordinate is the NPV in $MM. This curve shows the trade-off between economic performance and environmental conservancy.

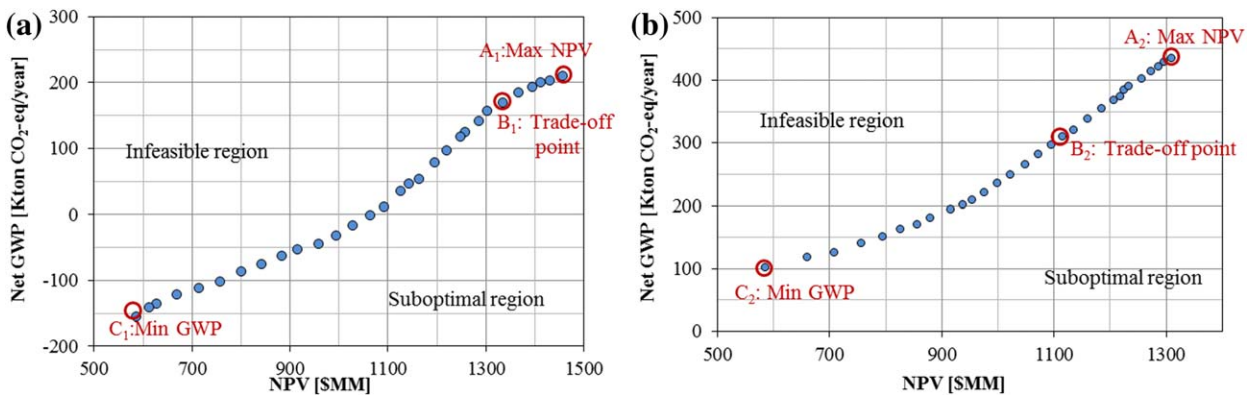

Figure 8. Pareto-optimal solutions of process design.

(a) LCSG scenario; (b) HCSG scenario. [Color figure can be viewed in the online issue, which is available at wileyonlinelibrary.com.]

Table 6. Overall Material/Energy Balances for the Pareto-Optimal Designs

	LCSG Scenario			HCSG Scenario		
	Maximum NPV (A_1)	Trade-off (B_1)	Minimum GWP (C_1)	Maximum 3NPV (A_2)	Trade-off (B_2)	Minimum GWP (C_2)
Consumption						
Shale gas (GJ/h)	2093	2093	2093	2093	2093	2093
Bioethanol(Gallon/h)	2,541	7,359	27,636	8,716	14,668	27,248
Electricity (MWh)	39.91	44.10	47.35	44.27	44.64	48.08
Cooling water (tons/h)[a]	887	1063	2023	1154	1464	2071
Refrigerant (Mw)	48.41	50.21	45.63	51.12	47.06	45.05
Solvent (kg/day)	4.23	4.21	3.70	4.32	3.87	3.68
SCOT H_2 (kg/day)	85.0	85.0	85.0	85.0	85.0	85.0
Yield						
SG-ethylene (ton/day)	578	562	352	565	481	343
Bioethylene (ton/day)	113	281	1209	367	661	1254
Propylene (ton/day)	37.75	37.68	29.65	37.91	33.86	28.86
Butanes (gallon/h)	1528	1528	1515	1546	1533	1527
Natural gasoline (gallon/h	1083	1083	1088	1089	1090	1093
Hydrogen (kg/h)	901	920	752	919	840	739
Sulfur (kg/h)	477	477	477	477	477	477
Electricity (MWh)[b]	50.14	42.50	45.92	36.96	49.96	53.18

[a]The recycling rate of cooling water is assumed to be 0.8.
[b]The yield of electricity includes the power generation in power plant unit and power recovered from the HEP network.

The points on this curve are all Pareto-optimal, indicating that the NPV is maximized with respect to the specified GWP limit. Solutions in the region above the curve are infeasible, whereas solutions in the region below the curve are feasible but suboptimal. Each point on the Pareto curve represents an optimal design and operation of the process.

For the LCSG scenario in Figure 8a, point A_1 on the upper right has the maximum NPV among all feasible solutions. For this design, essentially all (99.99%) of the methane and most (75.8%) of the fuel gas (process purges, waste, tail gas, and methane) are directly sent to the power plant. As a result, the net electricity generated is maximized to 10.23 MWh. Meanwhile, the NPV is \$1457.3 MM, the GWP is 211.2 kton CO_2-eq/year, the corresponding MESP is \$476.5/kg, and the unit GWP of ethylene is 0.119 kg CO_2-eq/kg. In contrast, point C_1 on the bottom left has the smallest GWP, where 79.50% of the fuel gas is used as dehydration fuel. Thus, the unit GWP and NPV decline to -154.6 kton CO_2-eq/year and \$585.1 MM, respectively. The corresponding MESP is \$ 1070.6/kg, and the unit GWP is -0.615 kg CO_2-eq/kg. A comparison between points A_1 and C_1 validates that bioethanol as a renewable fuel can play an important role in reducing the life cycle carbon footprint. Similarly, the high methane leaking factor of shale gas in the HCSG scenario leads to a unit GWP which is, on average, 0.5 kg CO_2-eq/kg higher than in the LCSG scenario, shown in Figure 8b. In this scenario, as the NPV decreases from \$1321.8 to \$577.7 MM, the annual GHG emissions reduces from 436.2 to 102.9 ktons CO_2-eq. In particular, the MESPs of the points A_2 and C_2 are \$712.2/kg and \$1075.8/kg, while their corresponding annual GHG emissions are 0.804 and -0.115 kton/CO_2-eq.

The process is designed to produce greener and more cost-effective chemicals from shale gas, and bioethanol is used as an auxiliary feedstock. Therefore, to locate a more reasonable point between the above extreme optimal points, two guidelines should be followed: GWP for unit ethylene produced (kgCO_2-eq/kg ethylene) should be lower than petroleum-based ethylene ($GWP_{E2E} < 1.70$[23]), and the amount of bioethanol should not exceed that of shale gas (bioethanol/SG < 1, on molar basis). Furthermore, note that from point A_1 (A_2) to point B_1 (B_2), the GWP_{E2E} is significantly reduced, while there is only a small rise of the MESP. This implies that the trade-off design of point B_1 (B_2) is a "good choice" solution.

Process yield and consumption

The process consumption of raw materials and energy, and the process yield for all optimal designs are given in Table 6. For given plant capacity of shale gas (2093 GJ/h input), the HCSG scenario requires on average 2.50 times more bioethanol feed higher than that of the LCSG scenario outside of the minimum GWP design. The minimum GWP design has the highest amount of bioethanol feed and bioethylene production. For example, 1209 kton/day of bioethylene is produced from the optimal design of point C_1, which is equivalent to 10.70 times and 4.30 times higher than in the optimal designs of point A_1 and point B_1, respectively. Note that, a high bioethanol feed rate in the minimum GWP design also increases water consumption by about 100%. This is because BD consumes the same amount of MP steam and bioethanol. Although the purification of crude bioethylene is a cooling-intensive process, the amount of refrigerant used in the minimum GWP design is lower than that used in the other optimal designs. The main reason is that in the minimum GWP design, a large amount of H_2-rich gas is rejected in the preseparator operating at -90.5 to 149.5°C (Table 2). The production of hydrogen extracted from H_2-rich gas supports this point, as listed in Table 6. Note that the H_2-rich gas with a low boiling point is more difficult to be liquefied than ethylene.

Figure 9 shows the breakdown of olefins production for the optimal designs of selected Pareto points. In this figure, a new reported CRD design[6] is used as a reference process which integrates shale gas processing with onsite ethylene production. Explicitly, the CRD design features better energy savings and equipment sharing by directly recycling the cracking gas to the dehydration unit. However, the Pareto-optimal designs for the proposed process can produce 5.00–10.90 times as many olefins as compared with the reference

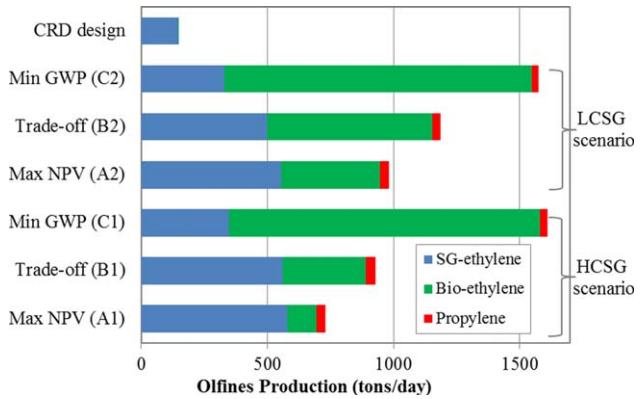

Figure 9. Comparison of olefins production among the Pareto-optimal designs and CRD design.[6]

[Color figure can be viewed in the online issue, which is available at wileyonlinelibrary.com.]

CRD design. The contribution comes from the integration of bioethylene production and OCM reaction. For both the HCSG and LCSG scenarios, the bioethylene contributes the largest share of olefins production in the minimum GWP designs (e.g., 77.5 wt % at point C_1 and 78.5 wt % at point C_2). But, this share drops substantially in the other optimal designs. For maximum NPV designs, the production of SG-ethylene is increased to 578 tons/day at point A_1 and 565 tons/day at point A_2, accounting for 83.6 and 60.6% of the total, respectively. Among the optimal designs, the propylene maintains a small capacity between 29.65 and 37.75 tons/day.

As shown in dark blue bars in Figure 10, although they all use the Eagle Ford shale gas as raw material, the Pareto-optimal design in the proposed process is more productive than the reference design. Given this result, we only select the trade-off design of point B_1 for comparison. For the CRD design, only 145 tons/day of ethylene is produced from ethane via the steam cracking process. With the same feedstock, the trade-off design (point B_1) produces 562 tons/day of SG-ethylene, 57.6% of which directly comes from the OCM reaction. Meanwhile, we note that the methane conversion rate and the yields of ethylene and ethane in the OCM reaction are 27.7 and 21.3%, under the optimal operating conditions listed in Table 4. The OCM reaction simultaneously generates 171 tons/day of ethane, recovered by the ethylene splitter in the olefins separation unit and then sent to the olefins production unit where it is converted into ethylene. This indirectly contributes about 38.6% to ethylene production in this design. In total, 416 tons/day of ethylene is converted from methane, accounting for 74.0% of total production. This implies that methane plays a significant role in improving ethylene production when the OCM reaction is integrated with the olefins cracking facility.

In the proposed process, significant high temperature waste heat is generated through the OCM and cocracking reactions. This provides an opportunity for heat integration and power generation, as visualized in the temperature-enthalpy diagram of Figure 11. We select two Pareto-optimal designs of points B_1 and B_2 for analysis. Note that the red dash represents the original hot curve. Those sections where the hot curve is above the cold one require heat engines. In total, the difference in the enthalpy changes between hot and cold curve are 83.53 MW in the LCSG scenario and 98.81 MW in the HCSG scenario. Accordingly, if we assume that 100% of enthalpy changes are recovered and converted into power via the Rankine cycles, the power generation of each scenario is 28.42 and 35.16 MWh. A relatively greater amount of power is generated in the HCSG scenario. This is because the OCM reaction is fed at a higher oxygen/methane ratio (0.322 mol/mol), promoting the generation of recoverable high-temperature waste heat from the partial combustion of methane. Additionally, the LCSG scenario requires higher cold utilities. The reason is that in the optimal design of point B_1, a higher quantity of SG-ethylene (562 tons/day) needs to be extracted in the NGLs cutting and olefins separation units using low temperature refrigerants.

Economic analysis

The project economics are listed in Table 7, where the capital cost and project revenue are both presented in detail. The maximum NPV (points A_1 and A_2) and trade-off (points B_1 and B_2) designs have a similar TPC ranging at around \$240 MM. The minimum GWP design has a TAC of \$605.13 MM at Pareto point C_1 and \$622.59 MM at Pareto point C_2, equivalent to 2.27–3.61 times that of the TAC of the maximum NPV design. This is because bioethanol is more expensive than shale gas, and the increase in bioethanol input will significantly increase the total fuel cost. Accordingly, the increasing expense of bioethanol is the dominant contributor to the growth of the TAC, which accounts for about 80.0% of the sum in the minimum GWP design. Although the production of bioethylene has multiplied, the increase in total project revenue is not proportional to the TAC.

Figure 12 presents the breakdown of total direct cost among the optimal designs. The direct cost in the proposed process comes from the four process areas and the HEP network. For all optimal designs, the direct cost is mostly dominated by methane-to-ethylene area followed by the gas-to-chemicals area. They respectively make up 32.7–38.2 and 34.6–37.4% of the total cost. In particular, both the OCM reactor and ASU in the methane-to-ethylene area are highly capital-intensive sections. A high methane input would greatly increase the installation cost of this process area, and further increase the TDC of the entire process. Therefore, for both scenarios, the maximum NPV and trade-off designs with higher methane inputs require 11.1–17.3% higher TDC than that of the minimum GWP design. The minimum TDCs are found in the minimum GWP designs which require

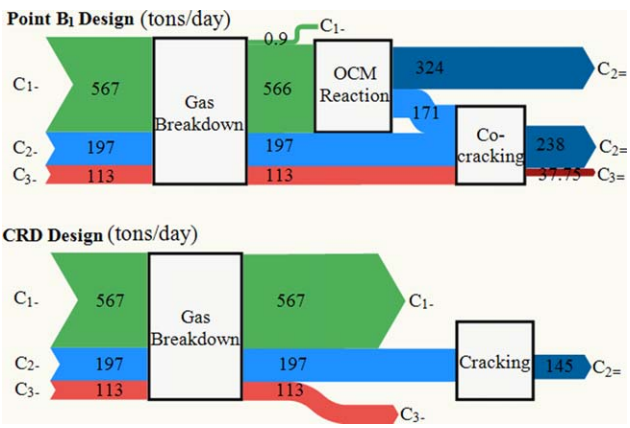

Figure 10. Carbon flow diagram of selected Pareto point B_1 design and CRD design[6] (ton/day).

[C_1-: methane, C_2-: ethane, C_3-: propane, C_2=: ethylene and C_3=: propylene]. [Color figure can be viewed in the online issue, which is available at wileyonlinelibrary.com.]

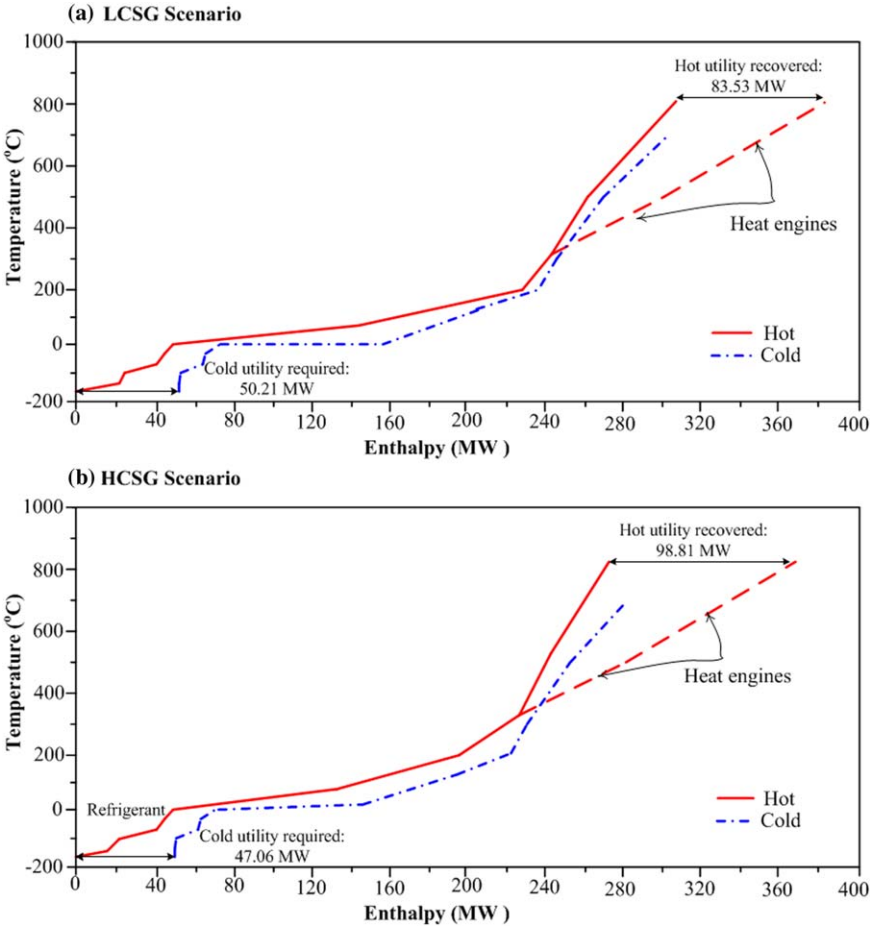

Figure 11. Temperature-enthalpy diagram of the optimal process for Pareto points B_1 and B_2.

(a) LCSG scenario; (b) HCSG scenario. [Color figure can be viewed in the online issue, which is available at wileyonlinelibrary.com.]

Table 7. Distributions of Capital Cost and Project Revenue (USD, $MM)

	LCSG Scenario			HCSG Scenario		
	Maximum NPV (A_1)	Trade-off (B_1)	Minimum GWP (C_1)	Maximum NPV (A_2)	Trade-off (B_2)	Minimum GWP (C_2)
Total direct cost (TDC)	183.85	185.30	157.91	183.49	179.77	161.72
Total installed cost (TIC)	153.21	154.41	131.59	152.91	149.81	134.77
Balance of plant cost (BOP)	30.64	30.88	26.32	30.58	29.96	26.95
Indirect cost (IC)	58.83	59.30	50.53	58.72	57.53	51.75
Total plant capital cost (TPC)	242.68	244.59	208.44	242.21	237.29	213.48
Total annual cost (TAC)	167.47	236.28	605.13	274.12	386.79	622.59
Capital recovery cost	16.31	16.44	14.01	16.28	15.95	14.35
Fuel cost (AFC)	137.74	204.56	575.62	238.97	356.69	593.58
a. Shale gas	92.41	92.41	92.41	92.41	92.41	92.41
b. Bioethanol	45.33	112.15	483.21	146.56	264.28	501.17
Nonfuel O&M cost (AOC)	13.42	15.28	15.50	18.87	14.15	14.66
a. Electricity	0	0.90	0.80	4.09	0	0
b. Cooling water	0.21	0.26	0.49	0.28	0.35	0.50
c. Refrigerant	12.90	13.82	13.91	14.19	13.43	13.86
d. Solvent ($\times 10^3$$)	5.64	5.61	4.93	5.60	5.17	4.90
e. CO_2 sequestration	0.30	0.30	0.29	0.31	0.37	0.30
Annual revenue (Rev)	349.87	405.18	686.33	441.20	525.11	703.31
SG-ethylene	231.20	224.80	140.80	226.00	192.40	137.20
Bioethylene	45.20	112.40	483.60	146.80	264.40	501.60
Propylene	16.86	16.83	13.24	16.94	15.13	12.89
Butanes	19.56	19.56	19.39	19.79	19.62	19.55
Natural gasoline	19.07	19.07	19.16	19.17	19.18	19.24
Net hydrogen	11.49	11.76	9.39	11.75	10.63	9.20
Sulfur	0.76	0.76	0.76	0.76	0.76	0.76
Electricity	5.73	0	0	0	2.98	2.86

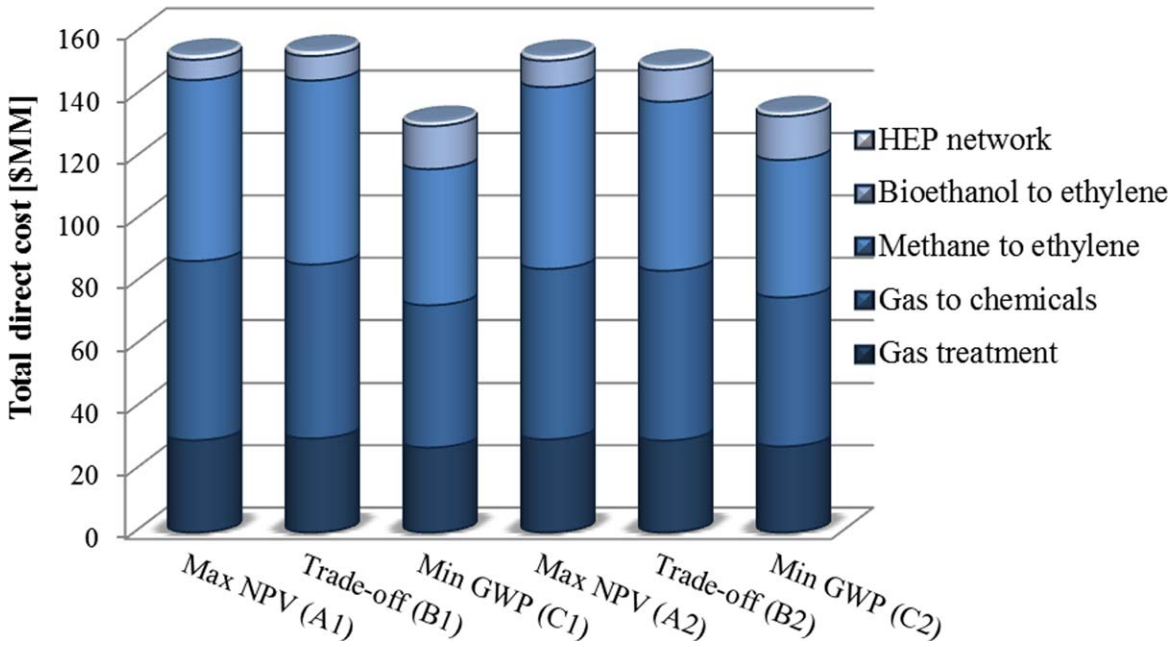

Figure 12. Total direct cost distribution among the optimal designs.

[Color figure can be viewed in the online issue, which is available at wileyonlinelibrary.com.]

$157.91 MM at Pareto point C_1 and $161.72 MM at Pareto point C_2.

Environmental impact analysis

Figure 13 illustrates the breakdown of the total GWP for the selected Pareto-optimal designs. Each horizontal bar in Figure 13 is divided into two parts. The positive part to the right of the vertical axis represents the GWP stemming from process operation, while the negtive part to the left represents the CO_2 credit from cultivating the biomass used to produce the bioethanol. It clearly shows that the highest contribution comes from the preparation of feedstocks including bioethanol and shale gas. The increase in the leaking factor of methane is the fundamental reason for the increase of GWP. Specifically, the GWP associated with shale gas preparation significantly increases from 156.1 kton CO_2-eq/year in the LCSG scenario to 442.2 kton CO_2-eq/year in the HCSG scenario. To enhance the overall sustainability, renewable bioethanol is used instead of fossil-derived fuels. As we move from the maximum NPV design to the minimum GWP design, the CO_2 credit (bioethanol-1) increases from 122.6 (396.4) to 1307.0 (1355.6) ktons/year in the LCSG (HCSG) scenario. However, the GHG emissions associated with bioethanol prepation (bioethanol-2) also increases proportionally from 71.3 (230.5) to 760.1 (788.3) ktons/year. The GHG emissons savings from bioethanol contribute to the sustainability of the entire process. In addtion, the electricity generation from the onsite power plant could also contribute to the decreasing of unit GWP of ethylene, such as the optimal design of point A_1. In this figure, the refrigerant also accounts for 5.0–17.0% of the total GWP. The remaining GWP contributors will be discussed below.

In addition to the carbon existing in the olefins and coproducts, the remaining carbon is mostly converted into CO_2 in this process. Figure 14 shows the breakdown of the total process CO_2 flow. In this figure, the SG-CO_2 is derived from the raw shale gas, while the OCM-CO_2 is from methane through the OCM reation. They are both compressed to supercritical pressures in the CO_2 compression unit. In this way, roughly 60% of process CO_2 will be sequestered for all optimal designs. The remaining process CO_2 is the source of direct CO_2 emissions, including the dehydration flue gas, power plant flue gas, and Claus flue gas. They account for 9.33–28.47, 9.19–28.28, and 0.60–0.93%, respectively, of the total, depending on the split ratios specified at points S_1 and S_2 (see Table 5). We note that the minimum GWP design generates the highest amount of process CO_2 with 283.08 kton/year in the LCSG scenario to 298.03 kton/year in the HCSG scenario. Accordingly, the direct CO_2 emission in fuel gas is increased to the highest share with about 60% of the total process CO_2. This is because relatively greater ratios of methane and fuel gas are used as dehydration fuels to maximize bioethylene production and minimize GWP.

$$\text{Cost of } CO_2 \text{ avoided } (\$/\text{kton}) = \frac{(\text{MESP})_{\text{reduction}} - (\text{MESP})_{\text{baseline}}}{(\text{GWP})_{\text{baseline}} - (\text{GWP})_{\text{reduction}}} \quad (32)$$

As previously mentioned, GHGs reduction operations including CCS and BD, contribute to GWP reduction. It is worthwhile to understand the costs behind these two

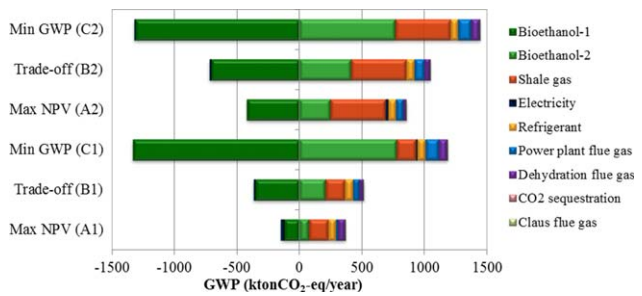

Figure 13. The distribution of GWP contribution for the selected Pareto points.

[Color figure can be viewed in the online issue, which is available at wileyonlinelibrary.com.]

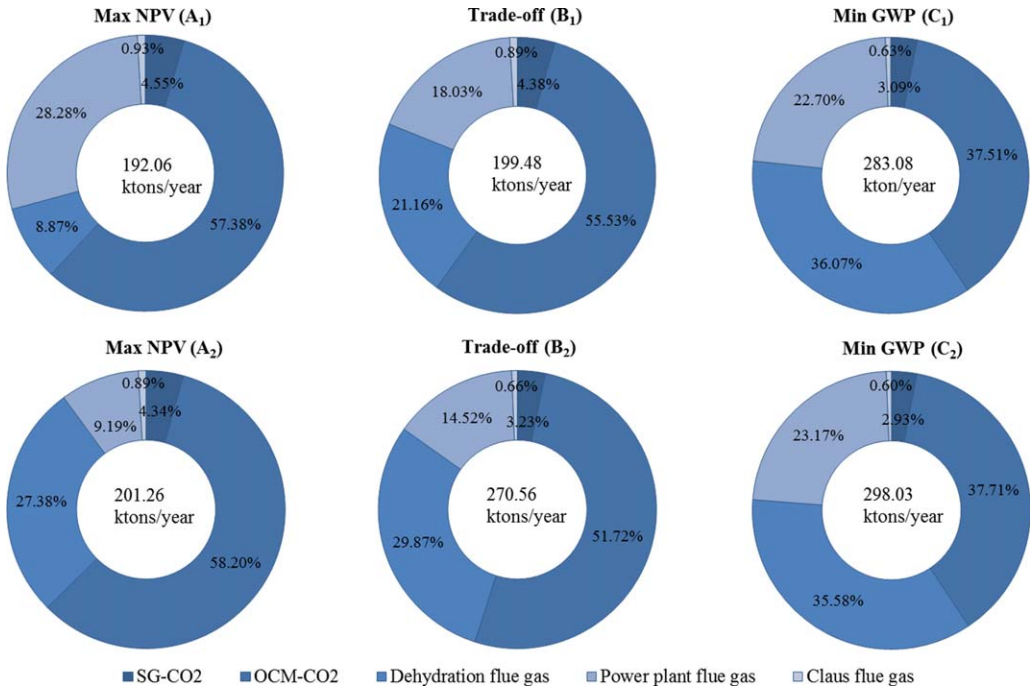

Figure 14. The distribution of overall CO_2 flow generated in the optimal designs.

The sources of direct CO_2 emissions include dehydration flue gas, power plant flue gas, and Claus flue gas, while the remaining gases are captured in this process. [Color figure can be viewed in the online issue, which is available at wileyonlinelibrary.com.]

operations. In this work, we investigate the joint or single effect of these operations, resulting in four options, listed in Table 8. For both scenarios, the sequence relationship of MESP is "BD+CCS" > "BD" > "CCS" > "no reduction." However, as for unit GWP, the sequence is reversed. In this work, we adopt the "CO_2 avoided cost" (see Eq. 32) indicator to measure the incremental MESP for a year divided by the difference in unit GWP between the baseline and reduction options. The results clearly show that, in the LCSG scenario, the CO_2 avoided cost is increased from \$102.7/kton for the CCS option to \$363.0/kton for the BD option. This indicates that the integration of BD is an expensive choice when shale is considered as a low carbon fuel. It should be noted in the HCSG scenario, however, that with CCS and no reduction options, the unit GWPs are 2.21 and 2.85 kg $CO_{2\text{-}eq}$/kg, respectively, both of which are less competitive than the petroleum-based pathway. In this case, the integration of BD becomes a necessary choice if we want to produce greener chemical. As listed in this table, the unit GWP can be significantly reduced to 0.720 kg $CO_{2\text{-}eq}$/kg for the BD option, and 0.360 kg $CO_{2\text{-}eq}$/kg for the BD+CCS option. Moreover, as we move from the LCSG scenario to the HCSG scenario, the CO_2 avoided cost has a sharp drop. The advantage in CO_2 avoided cost of the CCS option over that of the BD option decreases from 3.5 times to 2.3 times.

Sensitivity analysis of feedstocks

The quality of the raw shale gas, as determined by its composition, plays an important role in improving economic and environmental performances. In addition to Eagle Ford gas, two shale gases derived from Barnett formation[77] with superrich NGLs and Bakken formation[78] with rich NGLs are also evaluated in this work. The corresponding compositions are given in Table A1 in Appendix A. For a better comparison, the CGP (conventional shale gas processing plant without ethylene production) and CRD designs based on our previous work[6] are used as the reference designs. Uncertainty analysis is conducted to investigate the impact of feedstocks on the project economics. The uncertainty analysis used the Monte Carlo simulation method where we specify 20 uncertainty parameters including raw materials, products, and utilities as listed in Table 4. Moreover, the triangular distribution of TPC ranging from ±25% of the deterministic value listed in Table 7 is assumed in this model.

In Figure 15a, the forecast of NPV with 80% certainty is represented by the column with error bars located on the mean value. For the same gas feedstock, the optimal trade-off design exhibits the greatest estimated NPVs, which equals 2.12–5.75 times and 4.02–12.67 times the growth compared to the reference CRD and CGP designs, respectively. For the reference designs, the C_1 fraction (methane)

Table 8. Impacts of GWP Reduction Options on the Project Performances

	LCSG Scenario		HCSG Scenario		LCSG Scenario	HCSG Scenario
Reduction Option	MESP	GWP_{E2E}	MESP	GWP_{E2E}	CO_2 Avoided Cost	
BD+CCS	655.1	−0.03	877.2	0.360	252.0	197.6
BD	635.5	0.400	851	0.720	363.0	218.7
CCS	408.6	0.582	446.4	2.21	102.8	95.60
No reduction	345.1	1.20	385.2	2.85	Baseline	Baseline

For both two scenarios, the operating conditions are based on the optimal designs of points B_1 and B_2. Note that in the CCS option, the X_{S2} is equal to 0.

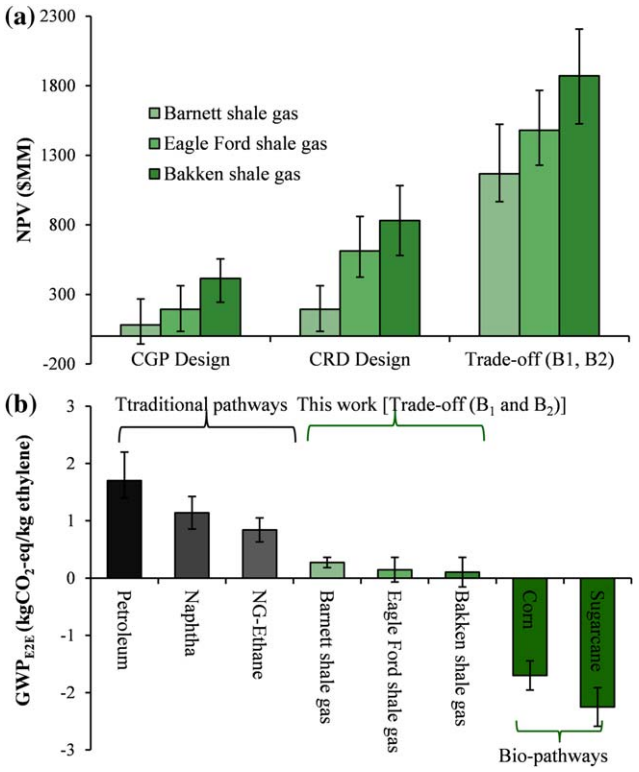

Figure 15. Impacts of feedstocks on economics and environment with error bars.

(a) project NPVs for different type of shale gas; (b) unit GWP of bioethylene and fossil ethylene. [Color figure can be viewed in the online issue, which is available at wileyonlinelibrary.com.]

is directly extracted from the raw gas and sold as pipeline gas. This leads to a serious lack of economic competitiveness with the NGLs-derived products. Thus, when the NGLs-leanest Barnett shale gas is used as a feedstock, the estimated NPVs of the CGP and CRD designs are only 19.42 and 23.18% of those of the designs fed by the NGLs-richest Bakken shale gas, respectively. But, the so-called "NGLs benefit" is weakened when methane is used as a new feedstock for chemicals production. For the optimal trade-off design, the estimated NPV based on Barnett shale gas is increased to 61.22% of that based on Bakken shale gas. This increment implies the integration with the OCM process can significantly improve the economic competitiveness of the C_1 fraction.

Figure 15b shows the comparison of unit GWP of ethylene produced from different feedstocks. Note that, for the CGP/CRD/trade-off designs, the upper and lower error bars located on the green columns represent the values estimated in the HCSG and LCSG scenarios. In this figure, as a new generation biofuel, it is no doubt that sugarcane is the most environmentally friendly feedstock for ethylene production with an average GWP_{E2E} of -2.25 kg CO_2-eq/kg, followed by corn with -1.70 kg CO_2-eq/kg of GWP_{E2E}.[23,72,73,79] In contrast, as a nonrenewable fuel, the petroleum-based pathway requires more energy to produce ethylene.[23,79] This results in the heaviest carbon footprint which is around 1.70 kg CO_2-eq/kg.[23,80] The unit GWPs for the steam cracking of naphtha and natural gas (NG)-derived ethane amount to 1.13 and 0.84 kg CO_2-eq/kg of ethylene.[80] On average, the corresponding GWP_{E2E} are 0.28, 0.16, and 0.11 kg CO_2-eq/kg for Barnett, Eagle Ford, and Bakken shale gases. Although they are still higher than the biopathways, the unit GWPs in trade-off designs are about 90.0, 83.5, 77.6% lower than those of the petroleum-based, naphtha-based, and NG-ethane-based pathways.

From an economic standpoint, the proposed process is more attractive than the biopathways. Currently, the production cost of lignocellulose-based ethylene is estimated at \$1900–2000/ton, and the lowest bioethylene production cost is around \$1200/ton based on a sugarcane feedstock in Brazil.[23] Meanwhile, the cost of petroleum-based ethylene is estimated at \$600–1300/ton depending on the region, with a global average of \$1100/ton.[23] In comparison, the MESP in trade-off designs ranges from \$622.4/ton to \$819.5/ton. These clearly indicate that the targets of greener and more cost-effective ethylene production are fulfilled simultaneously in the proposed process when compared to the traditional pathways and new biopathways.

Concluding Remarks

By combining the thermal conversion of C_1, C_2, and C_3 fractions in shale gas to ethylene and coproducts with renewable bioethylene production, significant production cost, and life cycle GHG emissions reductions are achieved compared to over previous process designs. Specifically, the integration of bioethylene production and CCS operation helps enhance the sustainability of the process. The high separation cost and project economics of the OCM process are mitigated by introducing a coprocessing strategy of OCM products, cocracking gas, and raw shale gas, and recovering OCM-derived ethane and methane efficiently. We formulate a systematic simulation-optimization framework that simultaneously achieves energy integration, and performs a techno-economic analysis and an environmental impact analysis. For a "good choice" optimal design, the MESP is \$655.1/ton and the unit GWP of ethylene (GWP_{E2E}) is 0.030 kg CO_2-eq/kg in the LCSG scenario, and \$877.2/ton and 0.360 kg CO_2-eq/kg in the HCSG scenario. The results reveal that, even considered as a high carbon feedstock in the HCSG scenario, shale gas can be converted to more cost-effective and greener chemicals.

Acknowledgments

The authors acknowledge financial support by Institute for Sustainability and Energy at Northwestern (ISEN). The authors thank Daniel Garcia, Jian Gong, and Jiyao Gao for their invaluable assistances to revise this article.

Notation

AFC = fuel cost
AOC = nonfuel operating and maintenance cost
BD = bioethanol dehydration
BEGP = break-even gas price
CSTRs = continuous stirred-tank reactors
CGP = conventional shale gas processing plant
CRD = on-site ethylene production design featured cracking gas recycling to dehydration unit
EPA = U.S. Environmental Protection Agency
FU = feedstocks and utilities
GHG = greenhouse gas
GWP = global warming potential
GTs/STs = gas turbines/steam turbines
HCs = hydrocarbons
HCSG = high carbon shale gas
HEP = heat exchange/power recovery

HRSG = heat recovery steam generator
IC = indirect cost
LCA = life cycle assessment
LCSG = low carbon shale gas
LP/MP/HP = high pressure/medium pressure/low pressure
LHV = low heating value
MESP = minimum ethylene selling price
NGLs = natural gas liquids
NPV = net present value
OCM = oxidative coupling of methane
PSA = pressure swing adsorption
K.O. = knock out
Rev = sales revenue
SCOT = shell Claus off-gas treating
WWT = waste water treatment

Sets/indices

E2E = ethylene
ele = electricity
out = outlet stream
sol = solvent including DEA, MDEA, and TEG
i^{H} = hot utility including hot water and HP/MP/LP steams
i^{C} = cold utility including cooling water and refrigerants
V = vapor stream
C = condenser
R = reboiler or reactor
L = liquid stream
In = inlet stream
0 = initial condition
ω = impact factor, $\omega \in (0,1]$

Parameters and variables

BPC = balance of plant cost, MM$
BOPF = balance of plant cost factor, %
F = mass flow rate, kg/h
Q = heat load, GJ/h
$Q^{U}_{i^H}$ = heat load of the hot utility stream i^{H}, GJ/h
$Q^{U}_{i^C}$ = heat cold of the hot utility stream i^{C}, GJ/h
$Q_{HX,k}$ = calculated heat load of the kth heat exchanger
$C^{U}_{i^H}$ = unit cost of hot utility i^{H}, $/GJ
$C^{U}_{i^C}$ = unit cost of cold utility i^{C}, $/GJ
R_k = heat residual from temperature interval k, GJ/h
C_{uti} = minimum utility cost, MM$
C_0 = basic equipment investment, MM$
X_{S_2}, X_{S_1} = distribution ratio at points S_1 and S_2, mole/mole
T_{OCM} = OCM temperature, °C
P_{OCM} = OCM pressure, bar
R_{O_2} = OCM O_2 feed (CH_4-M_4/S_1 inlet), mole/mole
R_{tax} = tax rate, %
r = discounted annual rate, %
T_{ccr} = cocracking temperature, °C
P_{ccr} = cocracking pressure, bar
T_{ls} = plant life span, year
T_{dp} = depreciation time, h
IC = indirect cost, MM$
ICF = indirect cost factor, %
IR = interest rate, %
TAC = total annual cost, MM$
TDC = total direct cost, MM$
TPC = total plant capital cost, MM$
η_k = overall energy efficiency of Rankine cycle in interval k, %
α_k = fraction of the hot composite stream from interval k used in the heat exchange network, GJ/h
δ_k = variable indicative of the presence of the hot utility in interval k
χ_k = variable indicative of the presence of the cold utility in interval k
γ_{SG,CH_4} = methane leakage/natural gas produced, v/v%
θ_{l,CO_2} = the equivalent amount of CO_2 emission associated with the production of l
$W_{HEP,k}$ = work generated from HEP network in interval k, kWh
$W_{con,k}$ = power needed for equipment j, kWh
$(F_{Cp,k})_{H,k}$ = the total heat transfer rate in composite curve in interval k, GJ/(°C s)
$(F_{Cp,k})_{C,k}$ = the total cold transfer rate in composite curve in interval k, GJ/(°C s)
$\Delta T_{min,H}/\Delta T_{min,H}$ = difference between the real temperature and scale temperature of the hot/cold streams, °C

Literature Cited

1. EIA. International Energy Outlook 2013: U.S. Energy Information Administration. 2013.
2. Scamuffa A, Lustig M, White T, McCutcheon RW, Gee G. *Shale Gas: Reshaping the US Chemicals Industry*. Los Angeles: Pricewaterhouse Coopers LLP, 2012.
3. Siirola JJ. The impact of shale gas in the chemical industry. *AIChE J*. 2014;60(3):810–819.
4. Armor JN. Emerging importance of shale gas to both the energy & chemicals landscape. *J Energy Chem*. 2013;22(1):21–26.
5. Rufford TE, Smart S, Watson GCY, Graham BF, Boxall J, Diniz da Costa JC, May EF. The removal of CO_2 and N_2 from natural gas: a review of conventional and emerging process technologies. *J Petrol Sci Eng*. 2012;94–95:123–154.
6. He C, You F. Shale gas processing integrated with ethylene production: novel process designs, exergy analysis, and techno-economic analysis. *Ind Eng Chem Res*. 2014;53(28):11442–11459.
7. Guo X, Fang G, Li G, Ma H, Fan H, Yu L, Ma C, Wu X, Deng D, Wei M, Tan D, Si R, Zhang S, Li J, Sun L, Tang Z, Pan X, Bao X. Direct, nonoxidative conversion of methane to ethylene, aromatics, and hydrogen. *Science*. 2014;344(6184):616–619.
8. Ehlinger VM, Gabriel KJ, Noureldin MMB, El-Halwagi MM. Process design and integration of shale gas to methanol. *ACS Sustain Chem Eng*. 2013;2(1):30–37.
9. Julián-Durán LM, Ortiz-Espinoza AP, El-Halwagi MM, Jiménez-Gutiérrez A. Techno-economic assessment and environmental impact of shale gas alternatives to methanol. *ACS Sustain Chem Eng*. 2014; 2:2338–2344.
10. Martín M, Grossmann IE. Optimal use of hybrid feedstock, switchgrass and shale gas for the simultaneous production of hydrogen and liquid fuels. *Energy*. 2013;55:378–391.
11. Keller GE, Bhasin M. Synthesis of ethylene via oxidative coupling of methane: I. *Determination of active catalysts*. *J Catal*. 1982;73(1):9–19.
12. Godini HR, Xiao S, Jašo S, Stünkel S, Salerno D, Son NX, Song S, Wozny G. Techno-economic analysis of integrating the methane oxidative coupling and methane reforming processes. *Fuel Process Technol*. 2013;106:684–694.
13. Eppinger T, Wehinger G, Kraume M. Parameter optimization for the oxidative coupling of methane in a fixed bed reactor by combination of response surface methodology and computational fluid dynamics. *Chem Eng Res Des* 2014;92:1693–1703.
14. Siluria Technologies I. Siluria & Braskem to explore deployment of Siluria's OCM technology for making ethylene from natural gas. *Focus Catal*. 2014;2014(4):6–7.
15. Weber CL, Clavin C. Life cycle carbon footprint of shale gas: review of evidence and implications. *Environ Sci Technol*. 2012; 46(11):5688–5695.
16. Newell RG, Raimi D. Implications of shale gas development for climate change. *Environ Sci Technol*. 2014;48(15):8360–8368.
17. Laurenzi IJ, Jersey GR. Life cycle greenhouse gas emissions and freshwater consumption of Marcellus shale gas. *Environ Sci Technol*. 2013;47(9):4896–4903.
18. Yang L, Grossmann IE, Manno J. Optimization models for shale gas water management. *AIChE J*. 2014;60:3490–3501.
19. Gao J, You F. Optimal design and operations of supply chain networks for water management in shale gas production: MILFP model and algorithms for the water-energy nexus. *AIChE J*. In press. DOI: 10.1002/aic.14705.
20. Brandt AR, Heath GA, Kort EA. Methane leaks from North American natural gas systems. *Science*. 2014;343(6172):733–735.
21. Howarth RW. A bridge to nowhere: methane emissions and the greenhouse gas footprint of natural gas. *Energy Sci Eng*. 2014;2(2):47–60.
22. He C, You F, Feng X. A novel hybrid feedstock to liquids and electricity process: process modeling and exergoeconomic life cycle optimization. *AIChE J*. 2014;60(11):3739–3753.
23. Broeren M. *Production of Bio-Ethylene-Technology Brief*. IEA-ETSAP & IRENA, International Renewable Energy Agency, 2013.

24. Yue DJ, You FQ, Snyder SW. Biomass-to-bioenergy and biofuel supply chain optimization: overview, key issues and challenges. *Comput Chem Eng*. 2014;66:36–56.
25. Haro P, Ollero P, Trippe F. Technoeconomic assessment of potential processes for bio-ethylene production. *Fuel Process Technol*. 2013; 114:35–48.
26. George DL, Bowles EB. Shale gas measurement and associated issues. *Oil Gas J*. 2011;238(7). Available at: http://www.pipelineandgasjournal.com/shale-gas-measurement-and-associated-issues.
27. Speight JG. Shale gas properties and processing. In: Speight JG, editor. *Shale Gas Production Processes, Chapter 4*. Boston: Gulf Professional Publishing, 2013:101–119.
28. Bahadori A, Vuthaluru HB, Mokhatab S. Method accurately predicts water content of natural gases. *Energy Source Part A*. 2009;31(9): 754–760.
29. Parks LE, Perry D, Fedich R. FLEXSORB ®SE A proven reliable acid gas enrichment solvent. In: Benyahia F, Eljack FT, editors. *Proceedings of the 2nd Annual Gas Processing Symposium, Vol. 2*. Amsterdam: Elsevier, 2010:229–235.
30. Siluria Technologies I, Inventor. Oxidative coupling of methane systems and methods. US Patent WO2013177433 A2, 2013.
31. Liu F. *Hydrogen Integration in Oil Refineries*. Manchester: Department of Process Integration, University of Manchester, 2002.
32. Wang H, Evans B, Goethem MV. Co-cracking Vs. segregated "hybrid" cracking in individual furnaces – design and operational considerations. *AIChE Spring Meeting and Global Congress on Process Safety*. Chicago, IL, 2011.
33. Mallapragada DS, Tawarmalani M, Agrawal R. Synthesis of augmented biofuel processes using solar energy. *AIChE J*. 2014;60(7): 2533–2545.
34. GREET. *The greenhouse gases, regulated emissions, and energy use in transportation model*. Oak Ridge, TN: Argonne National Laboratory, 2012.
35. Field RP, Brasington R. Baseline flowsheet model for IGCC with carbon capture. *Ind Eng Chem Res*. 2011;50(19):11306–11312.
36. Ecoinvent database Swiss Centre for Life Cycle Inventories. 2009. Accessed on August 28, 2014.
37. Holiastos K, Manousiouthakis V. Minimum hot/cold/electric utility cost for heat exchange networks. *Comput Chem Eng*. 2002;26(1):3–16.
38. Mokhatab S, Poe WA. Natural gas sweetening. In: Mokhatab S, Poe WA, editors. *Handbook of Natural Gas Transmission and Processing, 2nd Ed., Chapter 7*. Boston: Gulf Professional Publishing, 2012:253–290.
39. Bahadori A. Natural gas dehydration. In: Bahadori A, editor. *Natural Gas Processing, Chapter 9*. Boston: Gulf Professional Publishing, 2014:441–481.
40. Mokhatab S, Poe WA. Sulfur recovery and handling. In: Mokhatab S, Poe WA, editors. *Handbook of Natural Gas Transmission and Processing, Chapter 8, 2nd Ed*. Boston: Gulf Professional Publishing, 2012:291–316.
41. Bhattacharyya D, Turton R, Zitney SE. Steady-state simulation and optimization of an integrated gasification combined cycle power plant with CO_2 capture. *Ind Eng Chem Res*. 2010;50(3):1674–1690.
42. Froment GP, Van de Steene BO, Van Damme PS, Narayanan S, Goossens AG. Thermal cracking of ethane and ethane-propane mixtures. *Ind Eng Chem Process Des Dev*. 1976;15(4):495–504.
43. Froment GF, Van De Steene BO, Vanden Berghe PJ, Goossens AG. Thermal cracking of light hydrocarbons and their mixtures. *AIChE J*. 1977;23(1):93–106.
44. Jašo S, Godini HR, Arellano-Garcia H, Omidkhah M, Wozny G. Analysis of attainable reactor performance for the oxidative methane coupling process. *Chem Eng Sci*. 2010;65(24):6341–6352.
45. Stansch Z, Mleczko L, Baerns M. Comprehensive kinetics of oxidative coupling of methane over the La_2O_3/CaO catalyst. *Ind Eng Chem Res*. 1997;36(7):2568–2579.
46. Arvidsson M. *Process Integration Study of a Biorefinery Producing Ethylene from Lignocellulosic Feedstock for a Chemical Cluster*. Göteborg, Sweden: Chalmers University Of Technology, 2011.
47. Siemens Energy & Automation I. Composition Measurement in Ethylene Plants, 2012. Available at https://extranet.w3.siemens.com/us/internet-dms/ia/AppliedAutomation/AppliedAutomation/docs_ap/Ethylene.pdf. Accessed on July 24, 2014.
48. Deb K, Pratap A, Agarwal S. A fast and elitist multiobjective genetic algorithm: NSGA-II. *IEEE Trans Evol Comput*. 2002;6(2):182–197.
49. Yue DJ, Kim MA, You FQ. Design of sustainable product systems and supply chains with life cycle optimization based on functional unit: general modeling framework, mixed-integer nonlinear programming algorithms and case study on hydrocarbon biofuels. *ACS Sustain Chem Eng*. 2013;1(8):1003–1014.
50. Magazine CE. Chemical Engineering Plant Cost Index. 2014. Available at http://www.che.com/pci/. Accessed on August 2014.
51. Guillén-Gosálbez G, Caballero JA, Jiménez L. Application of life cycle assessment to the structural optimization of process flowsheets. *Ind Eng Chem Res*. 2008;47(3):777–789.
52. Zhang Q, Gong J, Skwarczek M, Yue DJ, You FQ. Sustainable process design and synthesis of hydrocarbon biorefinery through fast pyrolysis and hydroprocessing. *AIChE J*. 2014;60(3):980–994.
53. Grossmann IE, Guillen-Gosalbez G. Scope for the application of mathematical programming techniques in the synthesis and planning of sustainable processes. *Comput Chem Eng*. 2010;34(9):1365–1376.
54. Wang B, Gebreslassie BH, You F. Sustainable design and synthesis of hydrocarbon biorefinery via gasification pathway: integrated life cycle assessment and technoeconomic analysis with multiobjective superstructure optimization. *Comput Chem Eng*. 2013;52:55–76.
55. Gebreslassie BH, Slivinsky M, Wang BL, You FQ. Life cycle optimization for sustainable design and operations of hydrocarbon biorefinery via fast pyrolysis, hydrotreating and hydrocracking. *Comput Chem Eng*. 2013;50:71–91.
56. Gong J, You F. Global optimization for sustainable design and synthesis of algae processing network for CO_2 mitigation and biofuel production using life cycle optimization. *AIChE J*. 2014;60(9):3195–3210.
57. You FQ, Wang B. Life cycle optimization of biomass-to-liquid supply chains with distributed-centralized processing networks. *Ind Eng Chem Res*. 2011;50(17):10102–10127.
58. Gebreslassie BH, Waymire R, You FQ. Sustainable design and synthesis of algae-based biorefinery for simultaneous hydrocarbon biofuel production and carbon sequestration. *AIChE J*. 2013;59(5):1599–1621.
59. Garcia DJ, You F. Multiobjective optimization of product and process networks: general modeling framework, efficient global optimization algorithm, and case studies on bioconversion. *AIChE J*. In press. DOI: 10.1002/aic.14666.
60. Mearns E. What is the real cost of shale gas? 2013. Available at http://euanmearns.com/what-is-the-real-cost-of-shale-gas/. Accessed on August 28, 2014.
61. IPCC. *Carbon Dioxide Capture and Storage*. UK: Cambridge University Press, 2005.
62. AspenTech. *Aspen Process Economic Analyzer V7.2*. Burlington, MA: Aspen Technology, Inc., 2010.
63. Lynch E. *Compression and Dehydration of Carbon Dioxide for Oil Field Injection*. Argonne, IL: Argonne National Laboratory, ANL/CNSV-TM-158, 1985.
64. Vorgelegt V. *Optimal Synthesis of Downstream Processes using the Oxidative Coupling of Methane Reaction*. Berlin: Berlin Technical University, 2013.
65. Kreutz T, Williams R, Consonni S, Chiesa P. Co-production of hydrogen, electricity and CO_2 from coal with commercially ready technology. Part B: economic analysis. *Int J Hydrogen Energy*. 2005;30(7):769–784.
66. Holt N. IGCC power plants—EPRI design and cost studies. *Proceedings of EPRI/GTC Gasification Technologies Conference*. San Francisco, CA, 1998.
67. Gong J, You F. Value-added chemicals from microalgae: greener, more economical, or both? *ACS Sustain Chem Eng*. In press. DOI: 10.1021/sc500683w.
68. Gong J, You FQ. Optimal design and synthesis of algal biorefinery processes for biological carbon sequestration and utilization with zero direct greenhouse gas emissions: MINLP model and global optimization algorithm. *Ind Eng Chem Res*. 2014;53(4):1563–1579.
69. Hofstrand D. Greenhouse gas emissions of corn ethanol production. 2009. Available at http://www.agmrc.org/renewable_energy/climate_change/greenhouse-gas-emissions-of-corn-ethanol-production/. Accessed on August 1, 2014.
70. You FQ, Tao L, Graziano DJ, Snyder SW. Optimal design of sustainable cellulosic biofuel supply chains: multiobjective optimization coupled with life cycle assessment and input-output analysis. *AIChE J*. 2012;58(4):1157–1180.
71. Wildbolz C. *Life Cycle Assessment of Selected Technologies for CO_2 Transport and Sequestration*. Zurich, Switzerland: Swiss Federal Institute of Technology Zurich, 2007.
72. Howarth R, Santoro R, Ingraffea A. Methane and the greenhouse-gas footprint of natural gas from shale formations. *Clim Change*. 2011;106(4):679–690.
73. Clark C, Han J, Burnham A, Dunn J, Wang M. *Life-Cycle Analysis of Shale Gas and Natural Gas*. Argonne, IL: Argonne National Laboratory (ANL), 2012.

74. Gian-Kasper P, Stocker T, Midgley P, Tignor M. *IPCC Expert Meeting on the Science of Alternative Metrics*. Oslo, Norway: (IPCC) IPOCC, 2009.
75. Aspelund A, Gundersen T, Myklebust J, Nowak MP, Tomasgard A. An optimization-simulation model for a simple LNG process. *Comput Chem Eng*. 2010;34(10):1606–1617.
76. Kim IH, Dan S, Kim H, Rim HR, Lee JM, Yoon ES. Simulation-based optimization of multistage separation process in offshore oil and gas production facilities. *Ind Eng Chem Res*. 2014;53(21):8810–8820.
77. Hill RJ, Jarvie DM, Zumberge J, Henry M, Pollastro RM. Oil and gas geochemistry and petroleum systems of the Fort Worth Basin. *AAPG Bull*. 2007;91(4):445–473.
78. Woken CA, Stevens BG, Alemlie JC, Schlasner SM. *Enduse Technology Study - An Assessment of Alternative Uses for Associated Gas*. North Dakota Industrial Commission, 2013.
79. Alvarenga RAF, Dewulf J. Plastic vs. fuel: which use of the Brazilian ethanol can bring more environmental gains? *Renew Energy*. 2013;59:49–52.
80. Ghanta M, Fahey D, Subramaniam B. Environmental impacts of ethylene production from diverse feedstocks and energy sources. *Appl Petrochem Res*. 2014;4(2):167–179.

Appendix A

Table A1. Raw Shale Gas Composition

Eagle Ford		Bakken		Barnett	
Species	mol %	Species	mol %	Species	mol %
CH_4	74.25	CH_4	57.81	CH_4	85.45
C_2H_6	13.76	C_2H_6	19.98	C_2H_6	6.58
C_3H_8	5.4	C_3H_8	11.35	C_3H_8	1.92
i-C_4H_{10}	1.66	i-C_4H_{10}	0.96	i-C_4H_{10}	0.56
n-C_4H_{10}	1.11	n-C_4H_{10}	2.83	n-C_4H_{10}	0.75
i-C_5H_{12}	1.11	i-C_5H_{12}	0.38	i-C_5H_{12}	0.17
n-C_5H_{12}	0.55	n-C_5H_{12}	0.55	n-C_5H_{12}	0.13
C_6H_{14}	0.29	C_6H_{14}	0.22	C_6H_{14}	0
C_7H_{16}	0.1	C_7H_{16}	0.09	C_7H_{16}	0
C_8H_{18}	0.09	C_8H_{18}	0.04	C_8H_{18}	0
CO_2	1.52	CO_2	0.57	CO_2	1.66
N_2	0.16	N_2	5.22	N_2	2.78
H_2O	17.1, mg/scf	H_2O	32.2, mg/scf	H_2O	44.9, mg/scf
H_2S	307.2, mg/scf	H_2S	115.7, mg/scf	H_2S	335.3, mg/scf

Appendix B

Table B1. Expressions of Reaction Rate for Ethane–Propane Mixture[42,43]

No.	Reaction		Constant of Reaction Rate[a]	$A_{0,j}$ [1/s or 1/(mol s)[a]]	$E_{a,j}$ (kJ/mol)	Base Component
R(1)	$C_3H_8 \rightarrow C_2H_4+CH_4$		$A_{0,j}\times\mathrm{EXP}(-E_{a,j}/RT)$	$4.692\times\cdot10^{10}$	214.597	Propane
R(2)	$C_3H_8 \rightarrow C_3H_6+H_2$		$A_{0,j}\times\mathrm{EXP}(-E_{a,j}/RT)$	$5.888\times\cdot10^{10}$	214.597	Propane
R(3)	$C_3H_8+C_2H_4 \rightarrow C_2H_6+C_3H_6$		$A_{0,j}\times\mathrm{EXP}(-E_{a,j}/RT)$	$2.536\times\cdot10^{13}$	247.106	Propane
R(4)	$2C_3H_6 \rightarrow 3C_2H_4$		$A_{0,j}\times\mathrm{EXP}(-E_{a,j}/RT)$	$1.534\times\cdot10^{11}$	233.466	Propane
R(5)[a]	$6C_3H_6 \rightarrow 5\mathrm{Char}+3CH_4+2C_5H_{12}$		$A_{0,j}\times\mathrm{EXP}(-E_{a,j}/RT)$	$7.120\times\cdot10^{8}$	190.371	Propane
R(6)	$C_3H_6 \rightarrow C_2H_2+CH_4$		$A_{0,j}\times\mathrm{EXP}(-E_{a,j}/RT)$	$3.794\times\cdot10^{11}$	248.487	Propane
R(7)	$C_3H_6+C_2H_6 \rightarrow C_4H_8+CH_4$		$A_{0,j}\times\mathrm{EXP}(-E_{a,j}/RT)$	$1.000\times\cdot10^{14}$	251.081	
R(8)	$C_2H_6 \rightarrow C_2H_4+H_2$		$A_{0,j}\times\mathrm{EXP}(-E_{a,j}/RT)$	$4.652\cdot\times10^{13}$	272.796	Ethane
R(9)	$C_2H_4+C_2H_2 \rightarrow C_4H_6$		$A_{0,j}\times\mathrm{EXP}(-E_{a,j}/RT)$	$1.026\cdot\times10^{12}$	172.631	Ethane
R(10)	$C_2H_6+C_2H_4 \rightarrow C_3H_6+CH_4$		$A_{0,j}\times\mathrm{EXP}(-E_{a,j}/RT)$	$7.083\cdot\times10^{13}$	252.838	Ethane
Basis: wt %	CH_4	C_2H_6	C_2H_4	C_3H_6	C_3H_8	H_2
Result[b] (b^i_{mod})	13.75	22.02	42.80	12.56	5.86	3.01
Plant data (b^i_{ind})[42]	13.00	26.00	42.00	9.00	–	4.00
Relative error (RE, %)[c]	5.79	15.3	1.91	39.0	–	24.7

[a]The original reaction is $4C_3H_6 \rightarrow 6CH_4+C_{5+}$.[42] In the new R(5), pentane (C_5H_{12}) represents C_{5+} hydrocarbons.
Char is also considered in the equation in consistent with coke formation from propane (C_3H_6).
[b]Operating conditions: $T_{\mathrm{ccr}} = 750°\mathrm{C}$, $P_{\mathrm{ccr}} = 3.2$ bar, steam/ethane = 0.3 (mole basis), and ethane/propane = 1 (weight basis).
[c]$\mathrm{RE}=|b^i_{\mathrm{ind}}-b^i_{\mathrm{mod}}|/b^i_{\mathrm{ind}}\times100$.

Table B2. Expressions of Reaction Rate of OCM Reaction[45]

No.	Reaction	Constant of Reaction Rate[a]	$k_{0,j}$ [mol/(g s Pa^{m+n})]	$E_{a,j}$ (kJ/mol)	$K_{0,j}$ (Pa^{-1})	$k_{0,j}$ (kJ/mol)
R(1)	$CH_4 \rightarrow CO_2+2H_2O$	$\frac{k_{0,j}\times\mathrm{EXP}(-E_{a,j}/RT)\times p_{O_2}^{0.76}p_C^{0.24}}{[1+K_{j,CO_2}\times\mathrm{EXP}(-\Delta H_{ad,CO_2}/RT)\times p_{CO_2}]}$	$0.2\times\cdot10^{-5}$	48	$0.25\cdot\times10^{-12}$	−175
R(2)	$2CH_4+0.5O_2 \rightarrow C_2H_6+2H_2O$	$\frac{k_{0,j}\times\mathrm{EXP}(-E_{a,j}/RT)\times[0.23\times10^{-11}\mathrm{EXP}(-\Delta H_{ad,CO_2}/RT)]^{0.4}p_{CH_4}}{\{1+[0.23\times10^{-11}\times\mathrm{EXP}(-\Delta H_{ad,CO_2}/RT)\times p_{O_2}]^{0.4}+K_{j,CO_2}\times\mathrm{EXP}(-\Delta H_{ad,CO_2}/RT)\times p_{CO_2}\}^2}$	23.2	182	$0.83\times\cdot10^{-13}$	−186
R(3)	$CH_4+O_2 \rightarrow H_2O+CO+H_2$	$\frac{k_{0,j}\times\mathrm{EXP}(-E_{a,j}/RT)\times p_{O_2}^{0.85}p_C^{0.57}}{[1+K_{j,CO_2}\times\mathrm{EXP}(-\Delta H_{ad,CO_2}/RT)\times p_{CO_2}]}$	$0.52\cdot\times10^{-6}$	68	$0.36\times\cdot10^{-13}$	−187
R(4)	$CO+0.5O_2 \rightarrow CO_2$	$\frac{k_{0,j}\times\mathrm{EXP}(-E_{a,j}/RT)\times p_{O_2}^{0.55}p_C}{[1+K_{j,CO_2}\times\mathrm{EXP}(-\Delta H_{ad,CO_2}/RT)\times p_{CO_2}]}$	$0.11\cdot\times10^{-3}$	104	$0.40\times\cdot10^{-12}$	−168
R(5)	$C_2H_6+0.5O_2 \rightarrow C_2H_4+H_2O$	$\frac{k_{0,j}\times\mathrm{EXP}(-E_{a,j}/RT)\times p_{O_2}^{0.37}p_C^{0.95}}{[1+K_{j,CO_2}\times\mathrm{EXP}(-\Delta H_{ad,CO_2}/RT)\times p_{CO_2}]}$	0.17	157	$0.45\cdot\times10^{-12}$	−166
R(6)	$2O_2+C_2H_4 \rightarrow 2H_2O+2CO$	$\frac{k_{0,j}\times\mathrm{EXP}(-E_{a,j}/RT)\times p_{O_2}^{0.96}p_C}{[1+K_{j,CO_2}\times\mathrm{EXP}(-\Delta H_{ad,CO_2}/RT)\times p_{CO_2}]}$	0.06	166	$0.16\cdot\times10^{-12}$	−211
R(7)	$C_2H_6 \rightarrow C_2H_4+H_2$	$k_{0,j}\times\mathrm{EXP}(-E_{a,j}/RT)$	$1.2\cdot\times10^{7}$	226		
R(8)	$2H_2O+C_2H_4 \rightarrow 2CO+4H_2$	$k_{0,j}\times\mathrm{EXP}(-E_{a,j}/RT)\times p_C^{0.97}$	$9.3\cdot\times10^{3}$	300		
R(9)	$CO+H_2O \rightarrow CO_2+H_2$	$k_{0,j}\times\mathrm{EXP}(-E_{a,j}/RT)\times p_{O_2}p_C$	$0.19\cdot\times10^{-3}$	173		
R(10)	$CO_2+H_2 \rightarrow CO+H_2O$	$k_{0,j}\times\mathrm{EXP}(-E_{a,j}/RT)\times p_{O_2}p_C$	0.026	220		

[a]The original reaction is $4C_3H_6 \rightarrow 6CH_4+C_{5+}$.[42] In the new R(5), pentane (C_5H_{12}) represents C_{5+} hydrocarbons.

Appendix C

Convergence and computation time reduction

Combining the deterministic optimization with rigorous simulation significantly reduces the process noises and improves the accuracy of results.[75] However, the simulation model of this process contains large scale and complex equations including thermodynamic relations, fluid properties, kinetic reactions, equilibrium distillations and predefined unit operations (i.e., recycle, adjust, and set). In each iteration of the algorithm, almost all the computational time (>99.0%) is spent on running simulation. The computational efficiency is further constrained when the current MATLAB-HYSYS interface only allows a single simulation operation, although the experiment performed on a computer with multiple processors. Hence, parallel computation is impossible for this simulation-optimization approach, but may allow future discussion.

To obtain a feasible solution, we relax the related the constraints containing complex equations on the simulation model. The relaxation strategies are summarized in Table C1. First, the unit operations and process models with potentially demanding

Table C1. Relaxation Strategies of Constrains in Process Simulation[a]

(1) Unit Operation	Approach	
Recycle and Adjust 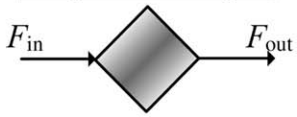	(1)reduce sensitivities (2) relax upper and lower bounds (3) increase step size (4) decrease tolerance (5) increase maximum iterations	
(2) Process Model [b]	**Replacement and approximation approach**	
Equilibrium-based distillation (CSTR/Plug flow) 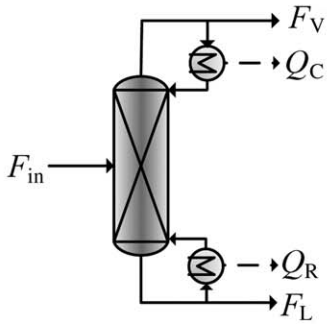	Component/shortcut separator 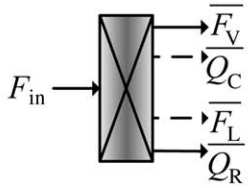	Mass balance $\overline{F_V} \approx F_V, \overline{F_V} \approx \overline{F_V}$ Energy balance $\overline{Q_C} \approx (\overline{F_V} / F_V^0)^{\omega} \times Q_C^0$ $\overline{Q_R} \approx (\overline{F_L} / F_L^0)^{\omega} \times Q_L^0$
Kinetic reactor (CSTR/Plug flow) 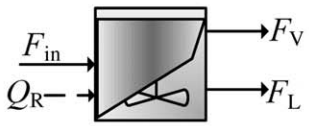	General reactor (Gibbs/conversion/equilibrium) 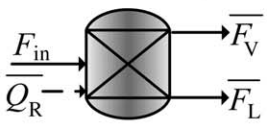	Mass balance $\overline{F_V} \approx F_V, \overline{F_V} \approx \overline{F_V}$ Energy balance $\overline{Q_R} \approx (\overline{F_V} / F_V)^{\omega} \times Q_R^0$
Multi-stream heat exchanger (heat exchanger/LNG exchanger/ fired heater/air cooler) 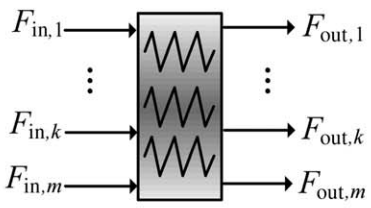	General heat exchanger (heater/cooler) 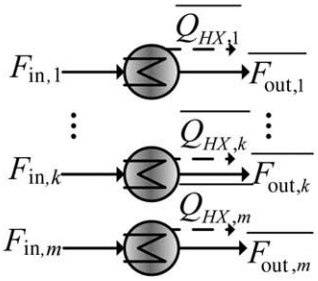	Mass balance $\overline{F_{out,1}} = F_{out,1}, \overline{F_{out,k}} = F_{out,k}$ $\overline{F_{out,m}} = F_{out,m}$ Energy balance $\overline{Q_{HX,1}} = 0, \overline{Q_{HX,k}} = 0$ $\overline{Q_{HX,m}} = 0$

[a]The nomenclature is provided in Notation.
[b]According to the proposed method, the demethanizer, ethylene splitter, and propylene splitter are all replaced by component separators in this work.

computational burden are identified from the entire process through possible troubleshooting. Typically, the most sensitive process models are equilibrium-based distillation, kinetic reactor, and multistream heat exchanger, and so forth. They are usually difficult to converge if the initial variables are changed. In next step, these rigorous models are replaced by the relaxed models in the model library. For example, a component separator can be considered as a reduced surrogate model to substitute for the equilibrium-based distillation. Specifically, the split ratios on the key components in the component separator are specified equal to the column component recoveries for the same component in the original distillation. As a result, the mass balances of outlets connecting to the surrogate model are approximately the same with that of the original outlets, while the energy balance is subject to an empirical relation. Finally, in case of unpredictable convergence problems, the constraints of the some unit operations (such as recycle and adjust) are simultaneously adjusted by providing tailored initial parameter settings.

Manuscript received Sept. 26, 2014, and revision received Nov. 28, 2014.